Vector meson-vector meson interaction in a hidden gauge unitary approach

L. S. Geng and E. Oset

Departamento de Física Teórica and IFIC, Universidad de Valencia-CSIC, E-46071 Valencia, Spain
(Received 11 December 2008; published 10 April 2009)

The formalism developed recently to study vector meson-vector meson interaction, and applied to the case of $\rho\rho$, is extended to study the interaction of the nonet of vector mesons among themselves. The interaction leads to poles of the scattering matrix corresponding to bound states or resonances. We show that 11 states (either bound or resonant) get dynamically generated in nine strangeness-isospin-spin channels. Five of them can be identified with those reported in the PDG, i.e., the $f_0(1370)$, $f_0(1710)$, $f_2(1270)$, $f_2'(1525)$, and $K_2^*(1430)$. The masses of the latter three tensor states have been used to fine-tune the free parameters of the unitary approach, i.e., the subtraction constants in evaluating the vector meson-vector meson loop functions in the dimensional regularization scheme. The branching ratios of these five dynamically generated states are found to be consistent with data. The existence of the other six states should be taken as predictions to be tested by future experiments.

I. INTRODUCTION

Although QCD has been generally accepted as the underlying theory of the strong interaction, due to the asymptotic freedom, its application at low energies around 1 GeV is highly problematic. Even in the case of lattice QCD, one still has to face many problems. Therefore, one often turns to various effective theories or models. Chiral symmetry, related with the small masses of u, d, s quarks, provides a general principle for constructing effective field theories to study low-energy strong-interaction phenomena. In this respect, chiral perturbation theory, χPT, has been rather successful in studies of low-energy hadronic phenomena [1–6]. See, for instance, Ref. [7] for a pedagogical introduction and Ref. [8] for recent developments in the one-baryon sector.

However, pure perturbation theory cannot describe the low-lying resonances. The breakthrough came with the application of unitary techniques in the conventional chiral perturbation theory, enabling one to study higher energy regions hitherto inaccessible, while employing chiral Lagrangians. The unitary extension of chiral perturbation theory, UχPT, has been successfully applied to study meson-baryon and meson-meson interactions. Several unitarization approaches have been developed over the years, including the inverse amplitude method [9,10], dispersion relations (the N/D method) [11,12], or in terms of coupled channel Bethe-Salpeter equation [13–15].

So far, the unitary chiral approach has been applied to study the self-interaction of the octet of pseudoscalars of the π [9,10,13,14,16], which provides the low-lying scalar mesons, the interaction of the octet of pseudoscalars of the π with the octet of baryons of the proton, which generates $J^P = 1/2^-$ baryonic resonances [12,15,17–21], the interaction of the octet of pseudoscalars of the π with the decuplet of baryons of the Δ [22,23], which leads to $J^P = 3/2^-$ baryon resonances, and the interaction of the octet of

pseudoscalars of the π with the nonet of vector mesons of the ρ, which leads to axial vector meson resonances [24,25]. These studies sometimes report "surprising" results, such as the existence of two $\Lambda(1405)$ states and two $K_1(1270)$ states. Both have found some experimental support [26,27]. This approach has also been extended to study systems including a heavy quark, charm or bottom, the so-called heavy-light systems [28–31], and to study three-body resonances [32,33].

The interaction of vector mesons with vector mesons or vector mesons with baryons has received little attention. One exception is the work of Ref. [34] where the vector-vector interaction is used to provide collision rates of vector mesons in heavy ion collisions. However, in a recent work [35], the task of finding bound states of $\rho\rho$ mesons was undertaken, using unitary techniques with the interaction vertices derived from the hidden-gauge Lagrangians [36,37]. Using as input the vertices provided by these Lagrangians and unitarizing the amplitudes via the Bethe-Salpeter equation, two poles were found on the complex plane: one in $(I, S) = (0, 0)$ and the other in $(I, S) = (0, 2)$ sector, which were identified with the $f_0(1370)$ and the $f_2(1270)$ states of the PDG [38]. The formalism provides naturally a stronger attraction for the tensor channel than for the scalar channel. A study of the radiative decays of these two states based on this approach has been performed [39].

The main purpose of the present paper is to extend the formalism developed in Ref. [35] to study vector meson-vector meson interaction in all possible strangeness-iso-spin-spin channels.

This paper is organized as follows: In Sec. II, we write down the hidden-gauge Lagrangians and briefly describe the several mechanisms that contribute to tree-level transition amplitudes, including four-vector-contact interaction, s, t, and u-channel vector exchange, and box diagrams that provide decays to two pseudoscalars. We

also explain in detail the approximations involved to make calculations feasible and the arguments supporting these approximations. In Sec. III, we look for poles on the complex plane and present results channel by channel. We show results both without and with the decay mechanism to two pseudoscalars. We also calculate the residues of these poles, which quantify the couplings of these states to different coupled channels and play a role in studies of their radiative decays. Section IV contains a brief summary and our main conclusions.

II. FORMALISM

In this work, as in Refs. [35,39], we use the Bethe-Salpeter equation method to unitarize the amplitudes. In this approach, the unitarized T amplitudes in coupled channels and s wave can be written as

$$T = V + VGT = (1 - VG)^{-1}V, \quad (1)$$

where V stands for the tree-level transition amplitudes, and G is a diagonal matrix with its element the vector meson-vector meson loop function

$$G = i \int \frac{d^4q}{(2\pi)^4} \frac{1}{q^2 - M_{V1}^2} \frac{1}{q^2 - M_{V2}^2}, \quad (2)$$

where M_{V1} and M_{V2} are the masses of the two vector-mesons.

As explained in Ref. [35] and also shown in Fig. 1, four possible mechanisms contribute to the tree-level transition amplitudes V: (1) four-vector-contact term [Fig. 1(a)]; (2) $t(u)$-channel vector meson exchange [Fig. 1(b)]; (3) s-channel vector meson exchange [Fig. 1(c)]; (4) box diagram with intermediate pseudoscalars (Fig. 1(d)). The corresponding diagram to the one in Fig. 1(d) with crossed pions was shown in Ref. [35] to provide much smaller contribution than the direct box diagram (Fig. 1(d)) for $\rho\rho$ scattering and, hence, we ignore it here. Similarly, in Ref. [35] the contribution of box diagrams with intermediate vector mesons involving anomalous couplings was also
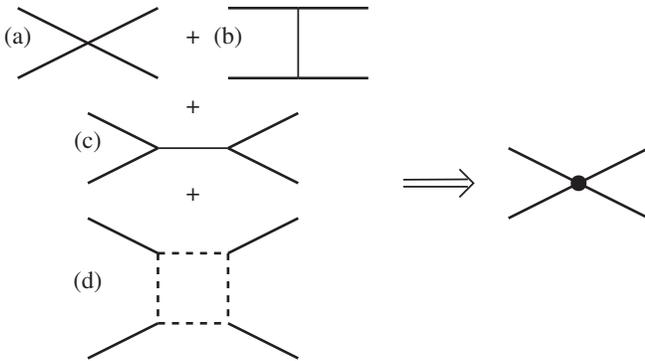

FIG. 1. The mechanisms contributing to the tree-level vertex of vector-vector scattering, which appears as V in the coupled channel Bethe-Salpeter equation.

found to be small and we shall also omit them in the present work.

In our approach, the first two diagrams play the most important role in the formation of resonances. The s-channel vector meson exchange is mostly of p-wave nature. In the case of the strangeness $= 1$ channel, an s-wave contribution appears, which is proportional to the differences between the initial (final) vector meson masses and is found to be numerically negligible compared to the sum of the contact mechanism and the $t(u)$-channel vector meson exchange mechanism. The box diagram depends somewhat on a form factor that we shall discuss later on. The real part of the amplitude is small compared to the sum of the four-vector-contact amplitude and the $t(u)$ channel vector-exchange amplitude, but the imaginary part is relatively large because there is a large phase space for the decay into two pseudoscalars, as has been explicitly shown in Ref. [35], where cancellations of the real part with that from the box diagram involving anomolous couplings was also found. Thus, we keep only its imaginary part.

We adopt the hidden-gauge formalism, consistent with chiral symmetry, to describe the interactions between the vector mesons and those between the vectors and the pseudoscalars [36,37]. The hidden-gauge Lagrangian is

$$\mathcal{L} = -\tfrac{1}{4}\langle \bar{V}_{\mu\nu}\bar{V}^{\mu\nu}\rangle + \tfrac{1}{2}M_v^2\langle[V_\mu - (i/g)\Gamma_\mu]^2\rangle, \quad (3)$$

where

$$\bar{V}_{\mu\nu} = \partial_\mu V_\nu - \partial_\nu V_\mu - ig[V_\mu, V_\nu],$$

$$\Gamma_\mu = \tfrac{1}{2}\{u^\dagger[\partial_\mu - i(v_\mu + a_\mu)]u + u[\partial_\mu - i(v_\mu - a_\mu)]u^\dagger\},$$

and $\langle\rangle$ stands for the trace in the SU(3) flavor space. V_μ represents the vector nonet

$$V_\mu = \begin{pmatrix} \frac{\omega+\rho^0}{\sqrt{2}} & \rho^+ & K^{*+} \\ \rho^- & \frac{\omega-\rho^0}{\sqrt{2}} & K^{*0} \\ K^{*-} & \bar{K}^{*0} & \phi \end{pmatrix}_\mu, \quad (4)$$

while $u^2 = U = \exp(\frac{i\sqrt{2}\Phi}{f})$ with Φ the octet of the pseudoscalars

$$\Phi = \begin{pmatrix} \frac{\eta}{\sqrt{6}} + \frac{\pi^0}{\sqrt{2}} & \pi^+ & K^+ \\ \pi^- & \frac{\eta}{\sqrt{6}} - \frac{\pi^0}{\sqrt{2}} & K^0 \\ K^- & \bar{K}^0 & -\sqrt{\frac{2}{3}}\eta \end{pmatrix}. \quad (5)$$

The value of the coupling constant g of the Lagrangian [Eq. (3)] is

$$g = \frac{M_V}{2f}, \quad (6)$$

with M_V the vector meson mass and $f = 93$ MeV the pion decay constant.

The Lagrangian of Eq. (3) provides the following two interactions:

$$\mathcal{L}_{VVVV} = \tfrac{1}{2}g^2\langle[V_\mu, V_\nu]V^\mu V^\nu\rangle, \qquad (7)$$

$$\begin{aligned}
\mathcal{L}_{VVV} &= ig\langle(\partial_\mu V_\nu - \partial_\nu V_\mu)V^\mu V^\nu\rangle \\
&= ig\langle V^\mu \partial_\nu V_\mu V^\nu - \partial_\nu V_\mu V^\mu V^\nu\rangle \\
&= ig\langle(V^\mu \partial_\nu V_\mu - \partial_\nu V_\mu V^\mu)V^\nu\rangle. \qquad (8)
\end{aligned}$$

The first one is responsible for the four-vector-contact interaction and the second one leads to the s, t, u-channel vector-exchange mechanisms.

To calculate the box diagram, one also needs the vector-pseudoscalar-pseudoscalar interaction, which is also provided by Eq. (3) as

$$\mathcal{L}_{V\Phi\Phi} = -ig\langle V_\mu[\Phi, \partial^\mu\Phi]\rangle. \qquad (9)$$

With the above vertices, one can then calculate the tree-level transition amplitudes for each strangeness and isospin channel. With the interaction of two spin-1 particles, the final state could have either spin 0, spin 1, or spin 2. One then has the following strangeness, isospin, and spin channels: (0, 0, 0), (0, 0, 1), (0, 0, 2), (0, 1, 0), (0, 1, 1), (0, 1, 2), (0, 2, 0), (0, 2, 1), (0, 2, 2), (1, 1/2, 0), (1, 1/2, 1), (1, 1/2, 2), (1, 3/2, 0), (1, 3/2, 1), (1, 3/2, 2), (2, 0, 0), (2, 0, 1), (2, 0, 2), (2, 1, 0), (2, 1, 1), and (2, 1, 2). In total, there are 21 channels. Proceeding further, we will see that not in all of these channels the vector meson-vector meson interaction leads to resonances.

An important ingredient in the Bethe-Salpeter equation method is the on-shell evaluation of the transition amplitudes V, which reduces the coupled channel integral equations to coupled channel algebraic equations. This can be justified using various methods, such as through a dispersion relation on T^{-1} after imposing unitarity [11,12], or in a more transparent way, writing $V(q^2) \simeq V(m^2) + \frac{\partial V}{\partial q^2} \times (q^2 - m^2)$. The off-shell part of the amplitude then cancels one vector meson propagator, leading to a tadpole kind of diagram. This diagram gets canceled with genuine tadpole diagrams from the same chiral Lagrangian, or, can be taken into account by redefining the couplings of the original transition amplitude. In any case, one can evaluate the transition amplitudes on shell.

Since we are only interested in the energy region close to the vector meson-vector meson threshold, one can safely ignore the three-momenta of the external vector mesons relative to their masses and, hence, the zero component of their polarization vectors. With the above mentioned on-shell factorization, as explained in detail in Ref. [35], one can prove that, after neglecting corrections of the order $|\vec{q}|^2/M_V^2$, the vector meson propagators in the loops of the Bethe-Salpeter series can be simplified as

$$\frac{\delta_{ij}}{q^2 - M_V^2 + i\epsilon}, \qquad (10)$$

with i, j the spacial indices of the polarization vectors. On the other hand, the propagator for the vector mesons ex-

changed in the t and u channels entering the evaluation of the tree-level transition amplitudes is given by

$$-g^{\mu\nu}\frac{1}{q^2 - M_V^2 + i\epsilon}. \qquad (11)$$

Within the approximations mentioned above of neglecting the three-momenta of the vector mesons versus their masses, the projection operators into spin 0, 1, and 2, in terms of the four polarization vectors, are [35]

$$\begin{aligned}
\mathcal{P}^{(0)} &= \tfrac{1}{3}\epsilon(1) \cdot \epsilon(2)\epsilon(3) \cdot \epsilon(4), \\
\mathcal{P}^{(1)} &= \tfrac{1}{2}[\epsilon(1) \cdot \epsilon(3)\epsilon(2) \cdot \epsilon(4) - \epsilon(1) \cdot \epsilon(4)\epsilon(2) \cdot \epsilon(3)], \\
\mathcal{P}^{(2)} &= \tfrac{1}{2}[\epsilon(1) \cdot \epsilon(3)\epsilon(2) \cdot \epsilon(4) + \epsilon(1) \cdot \epsilon(4)\epsilon(2) \cdot \epsilon(3)] \\
&\quad - \tfrac{1}{3}\epsilon(1) \cdot \epsilon(2)\epsilon(3) \cdot \epsilon(4). \qquad (12)
\end{aligned}$$

In the following, we explain how to calculate the three kinds of tree-level transition amplitudes, i.e., the four-vector-contact amplitude (Fig. 1(a)), the $t(u)$-channel vector-exchange amplitude (Fig. 1(b)), and the box amplitude (Fig. 1(d)).

A. Four-vector-contact term

With the spin projectors and the Lagrangian $\mathcal{L}_{VVVV}$, one can easily obtain the V_{ij}'s for different strangeness, isospin, and spin channels. The results for the strangeness $= 0$, isospin $= 0$ and spin $= 0$ channel can be found in Appendix A and those for other channels in the appendix of Ref. [40] (the arXiv version of the present paper). One thing to note is that for each pair of identical particles a factor of $\frac{1}{\sqrt{2}}$ has to be multiplied, i.e., the unitarity renormalization, which originates from the fact that

$$\frac{1}{2}\sum_q |I(\vec{q})I(-\vec{q})\rangle\langle I(\vec{q})I(-\vec{q})| = 1, \qquad (13)$$

where I denotes the identical particle [13]. One has to keep in mind that the unitarity renormalization has to be used to calculate the $t(u)$-channel vector-exchange diagrams and the box diagrams.

To obtain the amplitudes in isospin space, we use the following phase convention:

$$\rho^+ = -|1, +1\rangle, \qquad K^{*-} = -|1/2, -1/2\rangle. \qquad (14)$$

B. Vector exchange in $t(u)$ channel

To calculate the $t(u)$-channel vector meson exchange diagrams, one has to project the vertices into s wave. This can be done by the following replacements:

$$k_1 \cdot k_2 = \frac{s - M_1^2 - M_2^2}{2},$$

$$k_1 \cdot k_3 = k_1^0 k_3^0 - \vec{p} \cdot \vec{q} \rightarrow \frac{(s + M_1^2 - M_2^2)(s + M_3^2 - M_4^2)}{4s},$$

$$k_1 \cdot k_4 = k_1^0 k_4^0 + \vec{p} \cdot \vec{q} \rightarrow \frac{(s + M_1^2 - M_2^2)(s - M_3^2 + M_4^2)}{4s},$$

$$k_2 \cdot k_3 = k_2^0 k_3^0 + \vec{p} \cdot \vec{q} \rightarrow \frac{(s - M_1^2 + M_2^2)(s + M_3^2 - M_4^2)}{4s},$$

$$k_2 \cdot k_4 = k_2^0 k_4^0 - \vec{p} \cdot \vec{q} \rightarrow \frac{(s - M_1^2 + M_2^2)(s - M_3^2 + M_4^2)}{4s},$$

$$k_3 \cdot k_4 = \frac{s - M_3^2 - M_4^2}{2},$$

where $\rightarrow$ means the projection over s wave, and $k_1 = (k_1^0, \vec{p})$, $k_2 = (k_2^0, -\vec{p})$, $k_3 = (k_3^0, \vec{q})$, $k_4 = (k_4^0, -\vec{q})$ are the four-momenta of the particles 1, 2, 3, and 4 with masses M_1, M_2, M_3, and M_4.

The last expression of Eq. (8) is particularly suitable for the calculation of the vertices. Indeed, the vector field V^ν must correspond necessarily to the exchanged vector meson. If it were an external vector meson, the ν must be spatial as we mentioned and then ∂_ν leads to a three-momentum of an external vector, which is neglected in the present approach. Given the structure of the last expression in Eq. (8) one can easily see that all terms corresponding to the t channel $(1 + 2 \rightarrow 3 + 4)$ have the type

$$(k_1 + k_3) \cdot (k_2 + k_4)\epsilon_1 \cdot \epsilon_3 \epsilon_2 \cdot \epsilon_4, \tag{15}$$

while those corresponding to u-channel diagrams $(1 + 2 \rightarrow 4 + 3)$ have the structure

$$(k_1 + k_4) \cdot (k_2 + k_3)\epsilon_1 \cdot \epsilon_4 \epsilon_2 \cdot \epsilon_3. \tag{16}$$

It is interesting to note that the above structures of the $t(u)$ channel vector-exchange contributions, together with the structures of the projection operators [Eq. (12)], imply that they contribute equally to spin = 0 and spin = 2 states.

The resulting tree-level transition amplitudes for the strangeness = 0, isospin = 0, and spin = 0 channel are summarized in Appendix A and those for other channels can be found in the appendix of Ref. [40].

C. Box diagrams

The box diagrams provide a mechanism for the dynamically generated resonances to decay into two pseudoscalars. With the $\mathcal{L}_{V\Phi\Phi}$ Lagrangian of Eq. (9) and our assumption that the external particles have small three-momenta, these diagrams can be easily calculated, as shown in Ref. [35] and explained in the following.

The box diagrams have the following generic structure (with the notations shown in Fig. 2)
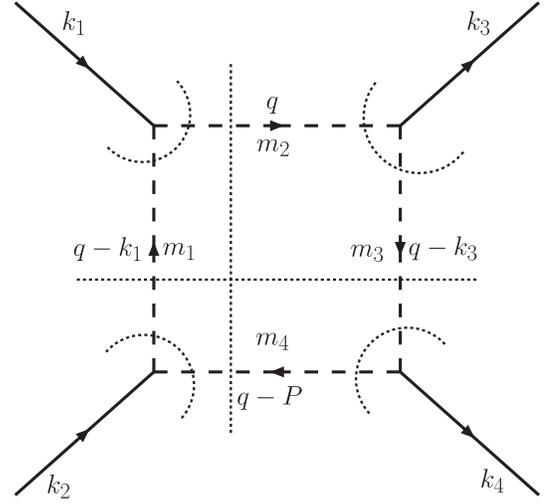

FIG. 2. Kinematics of a generic box diagram, with m_1, m_2, m_3, and m_4 denoting the masses of intermediate pseudoscalars and k_1, k_2, k_3, and k_4 the four-momenta of the vector particles.

$$V_b \sim C \int \frac{d^4 q}{(2\pi)^4} \epsilon_1 \cdot (2q - k_1)\epsilon_2 \cdot (2q - k_3)\epsilon_3$$

$$\cdot (2q - k_3 - P)\epsilon_4 \cdot (2q - k_1 - P)$$

$$\times \frac{1}{(q - k_1)^2 - m_1^2 + i\epsilon} \frac{1}{q^2 - m_2^2 + i\epsilon}$$

$$\times \frac{1}{(q - k_3)^2 - m_3^2 + i\epsilon} \frac{1}{(q - P)^2 - m_4^2 + i\epsilon}, \tag{17}$$

where C is the coupling of a certain transition. With the approximation of neglecting the three-momenta of the external particles, this can be simplified as

$$V_b \sim C' \int \frac{d^4 q}{(2\pi)^4} \epsilon_1^i \epsilon_2^j \epsilon_3^m \epsilon_4^n q^i q^j q^m q^n$$

$$\times \frac{1}{(q - k_1^0)^2 - m_1^2 + i\epsilon} \frac{1}{q^2 - m_2^2 + i\epsilon}$$

$$\times \frac{1}{(q - k_3^0)^2 - m_3^2 + i\epsilon} \frac{1}{(q - P^0)^2 - m_4^2 + i\epsilon}$$

$$= C'G, \tag{18}$$

with $C' = 16C$. To calculate this integral, we first integrate the q^0 variable by use of the residue theorem and close the integral below, as shown in Fig. 3, which leads to

$$G = (-2\pi i)\frac{1}{2\pi} \int \frac{d^3 q}{(2\pi)^3} \epsilon_1^i \epsilon_2^j \epsilon_3^m \epsilon_4^n q^i q^j q^m q^n \times \frac{G_n}{G_d}, \tag{19}$$
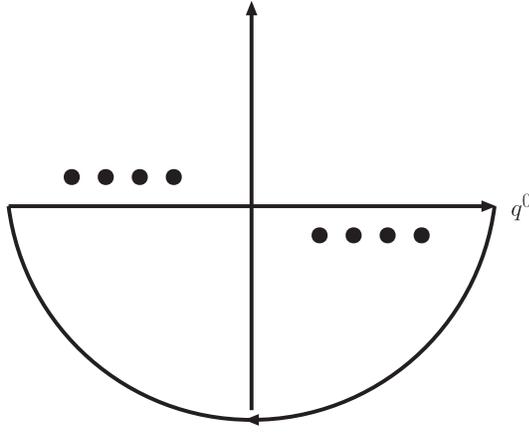
with

FIG. 3. The contour to evaluate a generic box diagram.

$$G_d = \frac{1}{2\omega_1\omega_2\omega_3\omega_4} \frac{1}{(-P^0 - \omega_2 - \omega_4)} \frac{1}{(k_1^0 + \omega_1 + \omega_2)}$$

$$\times \frac{1}{(k_3^0 + \omega_2 + \omega_3)} \frac{1}{(k_4^0 + \omega_3 + \omega_4)}$$

$$\times \frac{1}{(k_2^0 + \omega_1 + \omega_4)} \frac{1}{(k_1^0 - \omega_1 - \omega_2 + i\epsilon)}$$

$$\times \frac{1}{(k_3^0 - \omega_2 - \omega_3 + i\epsilon)} \frac{1}{(k_2^0 - \omega_1 - \omega_4 + i\epsilon)}$$

$$\times \frac{1}{(k_4^0 - \omega_3 - \omega_4 + i\epsilon)} \frac{1}{(P^0 - \omega_2 - \omega_4 + i\epsilon)}$$

$$\times \frac{1}{(k_1^0 - k_3^0 - \omega_1 - \omega_3 + i\epsilon)}$$

$$\times \frac{1}{(k_3^0 + k_1^0 - \omega_1 - \omega_3 + i\epsilon)},$$

where different cuts contributing to the imaginary part of the integral can be clearly seen (see also the dotted lines in Fig. 2), and $\omega_1 = \sqrt{q^2 + m_1^2}$, $\omega_2 = \sqrt{q^2 + m_2^2}$, $\omega_3 = \sqrt{q^2 + m_3^2}$, $\omega_4 = \sqrt{q^2 + m_4^2}$, $k_1^0 = \frac{s + M_1^2 - M_2^2}{2\sqrt{s}}$, $k_2^0 = \frac{s + M_2^2 - M_1^2}{2\sqrt{s}}$, $k_3^0 = \frac{s + M_3^2 - M_4^2}{2\sqrt{s}}$, $k_4^0 = \frac{s + M_4^2 - M_3^2}{2\sqrt{s}}$, and $P^0 = \sqrt{s}$, where m_1, m_2, m_3, and m_4 are the masses of intermediate pseudoscalars, M_1, M_2, M_3, and M_4 are the masses of the initial and final vector mesons, and $\sqrt{s}$ is the center of mass of energy of the vector-vector pair. G_n is also a function of these variables, whose explicit form is given in Appendix C.

Since

$$\int d^3q\, q_i q_j q_m q_n f(q)$$

$$= \frac{1}{15} \int d^3q\, q^4 f(q)(\delta_{ij}\delta_{mn} + \delta_{im}\delta_{jn} + \delta_{in}\delta_{jm}), \quad (20)$$

the four-point integral G becomes

$$G = (-i)\frac{1}{15}\frac{1}{2\pi^2} \int dq\, q^6 \frac{G_n}{G_d}$$

$$\times [\epsilon(1) \cdot \epsilon(2)\epsilon(3) \cdot \epsilon(4) + \epsilon(1) \cdot \epsilon(3)\epsilon(2) \cdot \epsilon(4)$$

$$+ \epsilon(1) \cdot \epsilon(4)\epsilon(2) \cdot \epsilon(3)]$$

$$= (-i)\frac{1}{15}\frac{1}{2\pi^2} \int dq\, q^6 \frac{G_n}{G_d} \times (5P^{(0)} + 2P^{(2)}). \quad (21)$$

As one can see from the above result, there is no contribution to spin $= 1$ channels from the box diagrams. This should be the case since two vectors in $L = 0$ have positive parity. To have $J = 1$ with two pseudoscalars one needs $L' = 1$ in the two pseudoscalars system, which, however, has negative parity. It is interesting to note that the box diagrams contribute 2.5 times more to the spin zero states than to the spin 2 states. This is one of the reasons why the scalar resonances develop a larger width than the tensor ones. The fact that the tensor resonances are more bound than the scalar ones reinforces this trend.

The explicit forms of the transition amplitudes are given in Appendix B with the following structure:

$$v_{i,j} = \sum cG_4(m_1, m_2, m_3, m_4, s, k_1^0, k_2^0, k_3^0, k_4^0),$$

$$+ \sum \tilde{c}\, G_4(m_1, m_2, m_3, m_4, s, k_1^0, k_2^0, k_4^0, k_3^0), \quad (22)$$

with c and $\tilde{c}$ the couplings and G_4 the four-point function defined as

$$G_4 = \frac{1}{15}\frac{1}{2\pi^2} \int dq\, q^6 \frac{G_n}{G_d}, \quad (23)$$

with G_d given in Eq. (20) and G_n given in the Appendix C.

As in Ref. [35], we evaluate the G_4 loop function with a cutoff of $\Lambda \sim 1$ GeV. To avoid the appearance of double poles, we replace the k_i^0's in the denominator G_d by

$$k_1^0 \to k_1^0 + \frac{\Gamma_1}{4}, \qquad k_3^0 \to k_3^0 - \frac{\Gamma_3}{4}, \quad (24)$$

$$k_2^0 \to k_2^0 + \frac{\Gamma_2}{4}, \qquad k_4^0 \to k_4^0 - \frac{\Gamma_4}{4}. \quad (25)$$

This was found to be a good approximation in Ref. [35] to the more accurate method of removing the double poles, which consists in making a convolution over the mass distributions of the external vector mesons to account for their widths.

We also multiply the vertices by the following form factors:

$$F_1(q^2) = \frac{\Lambda_b^2 - m_1^2}{\Lambda_b^2 - (k_1^0 - q^0)^2 + |\vec{q}|^2}, \quad (26)$$

$$F_3(q^2) = \frac{\Lambda_b^2 - m_3^2}{\Lambda_b^2 - (k_3^0 - q^0)^2 + |\vec{q}|^2}, \quad (27)$$

with $q^0 = \frac{s+m_2^2-m_4^2}{2\sqrt{s}}$, $\vec{q}$ the running variable, and $\Lambda_b = 1.4$ GeV [35]. These form factors are inspired by the fact that the largest piece of the imaginary part of G_4 comes from the cut at $P^0 = \omega_2 + \omega_4$ and inspired by the empirical form factors used in the decay of vector mesons [41,42]. The final form of the four-point function is then

$$G_4 = \frac{1}{15}\frac{1}{2\pi^2}\int_0^\Lambda dq\, q^6 \frac{G_n}{G_d} F_1(q^2)^2 F_3(q^2)^2. \quad (28)$$

Using the explicit expressions of $v_{i,j}$ of Eq. (22) in Appendix B, we can also calculate the partial decay widths into two pseudoscalars selecting only the particular channels. Technically, this implies keeping only the relevant terms in each $v_{i,j}$ of Appendix B. For instance, take the case of the strangeness $= 0$, isospin $= 0$, and spin $= 0$ channel as one example. If we want to have the $\pi\pi$ decay mode we keep only the terms that have m_π, m_π in the second and fourth arguments of each $\tilde{G}$ ($\tilde{G}(u)$) function.

III. RESULTS AND DISCUSSIONS

Since the vector mesons, particularly the ρ and the K^*, are rather broad, one has to take into account their widths. We follow Ref. [35] and convolute the vector-vector G function with the mass distributions of the two vector mesons, i.e., by replacing the G function appearing in the Bethe-Salpeter equation [Eq. (2)] by $\tilde{G}$

$$\tilde{G}(s) = \frac{1}{N^2}\int_{(M_1-2\Gamma_1)^2}^{(M_1+2\Gamma_1)^2} d\tilde{m}_1^2\left(-\frac{1}{\pi}\right)\mathrm{Im}\frac{1}{\tilde{m}_1^2 - M_1^2 + i\tilde{\Gamma}_1\tilde{m}_1}$$
$$\times \int_{(M_2-2\Gamma_2)^2}^{(M_2+2\Gamma_2)^2} d\tilde{m}_2^2\left(-\frac{1}{\pi}\right)\mathrm{Im}\frac{1}{\tilde{m}_2^2 - M_2^2 + i\tilde{\Gamma}_2\tilde{m}_2}$$
$$\times G(s, \tilde{m}_1^2, \tilde{m}_2^2), \quad (29)$$

with

$$N^2 = \int_{(M_1-2\Gamma_1)^2}^{(M_1+2\Gamma_1)^2} d\tilde{m}_1^2\left(-\frac{1}{\pi}\right)\mathrm{Im}\frac{1}{\tilde{m}_1^2 - M_1^2 + i\tilde{\Gamma}_1\tilde{m}_1}$$
$$\times \int_{(M_2-2\Gamma_2)^2}^{(M_2+2\Gamma_2)^2} d\tilde{m}_2^2\left(-\frac{1}{\pi}\right)\mathrm{Im}\frac{1}{\tilde{m}_2^2 - M_2^2 + i\tilde{\Gamma}_2\tilde{m}_2},$$

where M_1, M_2, Γ_1, and Γ_2 are the masses and widths of the two vector mesons in the loop. We only take into account the widths of the ρ and the K^*. In the case of the ω or ϕ, one or both of the kernels of these integrals will reduce to a delta function $\delta(\tilde{m}^2 - M^2)$. The $\tilde{\Gamma}_i$ function is energy dependent and has the form of

$$\tilde{\Gamma}(\tilde{m}) = \Gamma_0 \frac{q_{\mathrm{off}}^3}{q_{\mathrm{on}}^3}\Theta(\tilde{m} - m_1 - m_2), \quad (30)$$

with

$$q_{\mathrm{off}} = \frac{\lambda(\tilde{m}^2, m_\pi^2, m_\pi^2)}{2\tilde{m}}, \qquad q_{\mathrm{on}} = \frac{\lambda(M_\rho^2, m_\pi^2, m_\pi^2)}{2M_\rho} \quad (31)$$

and $m_1 = m_2 = m_\pi$ for the ρ or

$$q_{\mathrm{off}} = \frac{\lambda(\tilde{m}^2, m_K^2, m_\pi^2)}{2\tilde{m}}, \qquad q_{\mathrm{on}} = \frac{\lambda(M_{K^*}^2, m_K^2, m_\pi^2)}{2M_{K^*}}, \quad (32)$$

$m_1 = m_\pi$ and $m_2 = m_K$ for the K^*, where λ is the Källen function, $\lambda(x, y, z) = (x - y - z)^2 - 4yz$, and Γ_0 is the nominal width of the ρ or the K^*.

To regularize the loop functions, one can use either the cutoff method with a natural cutoff of ~ 1 GeV or the dimensional regularization method with $a \sim -2$ for meson-baryon scattering [12]. This means that by using these parameter values one should get the basic physics, providing a global description of the resonances generated dynamically in the approach. This is indeed the case here. Yet, in order to take into account possible correcting terms in the approach, we perform a fine-tuning of these parameters, such as to get a few resonances more precisely. Then, the results for other resonances are predictions. In practice, we adopt the following three-steps approach:

(1) First we use the cutoff method with $\Lambda \sim 1$ GeV to obtain the amplitudes on the real axis.

(2) Once peaks and bumps are observed, and persist with reasonable changes of the value of the cutoff Λ, we then use the dimensional regularization method with $\mu = 1000$ MeV and a adjusted to reproduce the cutoff results. More specifically, we reproduce the real part of the rho-rho loop function at the two ρ threshold. This gives $a = -1.65$.

(3) Then we fine-tune the a's for different isospin channels to fix the masses of some well-known resonances. In the present work, we use the masses of the $f_2(1270)$, the $f_2'(1525)$, and the $K_2^*(1430)$ for this purpose. This leads to $a_{\rho\rho} = -1.636$, $a_{K^*\bar{K}^*} = -1.726$, $a_{\rho K^*} = -1.85$. For the rest of the channels involving ω or ϕ, in the strangeness $= 0$ channel we use $a_i = a_{\rho\rho} = -1.65$; in the strangeness $= 1$ channel we use $a_i = a_{\rho K^*} = -1.85$; and in the strangeness $= 2$ channel, we use $a_i = a_{K^*\bar{K}^*} = -1.726$. These channels play a secondary role and moderate changes of these parameters barely affect the results. Hence, in practice, we are fine-tuning three parameters.

We should mention that our main conclusions would remain the same if we had used, for instance, the same value of $a_i = -1.85$ for all the channels, and we find only moderate changes in the masses of the resonances. For instance, with this choice of a_i, we would obtain the $f_2(1270)$ at $(1206, -i0)$ MeV on the complex plane without including the box diagrams, compared to $(1275, -i1)$ MeV with the fine-tuned subtraction constants, and the $1^-(0^{++})$ state at $(1770, -i50)$ MeV instead of $(1780, -i66)$ MeV (see Tables I and II). This means that we get the bulk of the resonances using a natural subtraction con-

TABLE I. Pole positions and residues in the strangeness = 0 and isospin = 0 channel. All quantities are in units of MeV.

	$K^*\bar{K}^*$	$\rho\rho$	$\omega\omega$	$\omega\phi$	$\phi\phi$
	$(1512, -i26)$ [spin = 0]				
g	$(1208, -i419)$	$(7920, -i1071)$	$(-39, i31)$	$(33, -i43)$	$(12, i24)$
	$(1726, -i14)$ [spin = 0]				
g	$(7124, i96)$	$(-1030, i1086)$	$(-1763, i108)$	$(3010, -i210)$	$(-2493, -i204)$
	$(1802, -i39)$ [spin = 1]				
g	$(8034, -i2542)$	0	0	0	0
	$(1275, -i1)$ [spin = 2]				
g	$(4733, -i53)$	$(10\,889, -i99)$	$(-440, i7)$	$(777, -i13)$	$(-675, i11)$
	$(1525, -i3)$ [spin = 2]				
g	$(10\,121, i101)$	$(-2443, i649)$	$(-2709, i8)$	$(5016, -i17)$	$(-4615, i17)$

stant (cutoff) for the effective field theory. Once this is done, fine-tuning of parameters will provide a better description of these resonances. Since we get 11 dynamically generated resonances and have fine-tuned three parameters to get the masses of the three resonances, we are making predictions for eight of them.

As to the total widths of the resonances, they are sensitive to the form factors given in Eqs. (26) and (27). The form factors used were inspired by the study of Refs. [41,42] and the precise value for Λ_b was taken from the study of Ref. [35]. Later in this section we mention the sensitivity of the widths to changes in the Λ_b value. Once again we can invoke the same fine-tuning strategy discussed above and say that a certain value of Λ_b is taken to get the total width of one of the fitted resonances, such that the widths of the others are predictions.

We should also note that the couplings of the resonances to the coupled channels are rather independent of the Λ_b parameter, which was already found in Ref. [39].

Finally, let us mention that our approach also predicts branching ratios to different channels. The

TABLE II. The same as Table I, but for the strangeness = 0 and isospin = 1 channel.

	$K^*\bar{K}^*$	$\rho\rho$	$\rho\omega$	$\rho\phi$
	$(1780, -i66)$ [spin = 0]			
g	$(7525, -i1529)$	0	$(-4042, i1391)$	$(4998, -i1872)$
	$(1679, -i118)$ [spin = 1]			
g	$(1040, -i1989)$	$(6961, -i4585)$	0	0
	$(1569, -i16)$ [spin = 2]			
g	$(10\,208, -i337)$	0	$(-4598, i451)$	$(6052, -i604)$

parameters of the approach have not been fine-tuned to these observables and, hence, all the branching ratios obtained are genuine predictions of our approach, which seem to be consistent with data as shown in the following sections.

The combination of the cutoff method and the dimensional regularization method has the following advantage: The use of the cutoff method is physically more transparent: the value of the cutoff should be around 1 GeV in order for the results to make sense. The use of the dimensional regularization method, on the other hand, enables one to go to the second Riemann sheet to obtain the pole positions and the residues. The results shown below are obtained in the dimensional regularization scheme. For the masses and widths of the vector mesons, we use the following values [38]: $M_\rho = 775.49$ MeV, $\Gamma_\rho = 149.4$ MeV, $M_{K^*} = 893.83$ MeV, $\Gamma_{K^*} = 50.55$ MeV, $M_\omega = 782.65$ MeV, $M_\phi = 1019.455$ MeV. For the masses of the pseudoscalars, the following values are used: $m_\pi = 138.04$ MeV, $m_K = 495.66$ MeV, $m_\eta = 547.51$ MeV [38]. The coupling constant $g = \frac{M_V}{2f}$ is evaluated with $M_V = M_\rho$ and $f = 93$ MeV. Of course, one could also use an averaged mass for M_V and an averaged f. In this case, both the numerator and the denominator will become somewhat larger, and the ratio is only slightly changed. Otherwise, in the potentials and in the $G(s)$ functions we have used the physical masses of the particles, as mentioned above. This, in particular, the large ϕ and ρ mass difference, introduces a certain source of SU(3) breaking, which might not be the only one present in the problem. However, the consideration of the physical masses is absolutely necessary to guarantee unitarity in coupled channels and to respect the positions of the thresholds, and this is the main reason to stick to physical masses in our approach.

The free parameters are then the subtraction constants used to regularize the vector-vector loop functions. In fact, the values can be different for each isospin channel, and

TABLE III. The same as Table I, but for the strangeness = 1 and isospin = 1/2 channel.

		$(1643, -i24)$ [spin $= 0$]	
	ρK^*	$K^* \omega$	$K^* \phi$
g	$(8102, -i959)$	$(1370, -i146)$	$(-1518, i209)$
		$(1737, -i82)$ [spin $= 1$]	
	ρK^*	$K^* \omega$	$K^* \phi$
g	$(7261, -i3284)$	$(1529, -i1307)$	$(-1388, i1721)$
		$(1431, -i1)$ [spin $= 2$]	
	ρK^*	$K^* \omega$	$K^* \phi$
g	$(10\,901, -i71)$	$(2267, -i13)$	$(-2898, i17)$

may even be different for different spins, but only slight changes can be expected [35]. Since the main purpose of this paper is to extend the work of Ref. [35] and to see whether in other strangeness-isospin-spin channels resonances can be dynamically generated, we do not use that freedom to fine-tune all the subtraction constants, which only leads to small changes in the masses of the resonances obtained.

In the following, we present our results channel by channel and compare with available data. We plot results for $|T|^2$ for different amplitudes, and in addition, we calculate the pole position and residues of the pole, which are presented in Tables I, II, and III. In the absence of the box diagrams, one can easily go to the complex plane. Around the pole position, the amplitude can be approximated by

$$T_{ij} = \frac{g_i g_j}{s - s_{\text{pole}}}, \tag{33}$$

where g_i (g_j) are the couplings to channel i (j).

The resonance parameters can be obtained from both the pole positions on the complex plane and the amplitudes squared on the real axis, as explained in the caption of Table IV. In Table IV, we summarize the resonance parameters for the dynamically generated states obtained both ways. Available data [38] are also given for comparison. All the results including the box diagrams shown in this paper are calculated with $\Lambda_b = 1.4$ GeV [see Eqs. (26) and (27)], unless otherwise stated. On the other hand, in Table IV, we also provide the resonance parameters calculated with $\Lambda_b = 1.5$ GeV. The comparison with those calculated with $\Lambda_b = 1.4$ GeV serves to quantify the uncertainties inherent in the calculation of the box diagrams, which provides a mechanism for the resonances to decay into two pseudoscalars.

A. Strangeness $= 0$ and Isospin $= 0$

In Fig. 4, all the $|T_{ii}|^2$'s for the strangeness $= 0$ and isospin $= 0$ channel are shown as a function of the invariant mass of the vector-vector pair. The upper, middle, and bottom panels show the results for spin $= 0$, spin $= 1$, and spin $= 2$ channels. Since the box diagrams only contribute to spin $= 0$ and spin $= 2$ channels, there are two plots in each panel for these spin channels. The left one shows the results without including the box diagrams, while the right one shows the results including the box diagrams. The comparison gives us an idea of the partial decay widths of the dynamically generated resonances decaying into two pseudoscalars. It should be noted that because we only consider the imaginary parts of the box diagrams, the pole positions on the real axis are almost the same in the two plots.

TABLE IV. The properties, (mass, width) [in units of MeV], of the 11 dynamically generated states and, if existing, of those of their PDG counterparts. Theoretical masses and widths are obtained from two different ways: "pole position" denotes the numbers obtained from the pole position on the complex plane, where the mass corresponds to the real part of the pole position and the width corresponds to 2 times the imaginary part of the pole position (the box diagrams corresponding to decays into two pseudoscalars are not included); "real axis" denotes the results obtained from real axis amplitudes squared, where the mass corresponds to the energy at which the amplitude squared has a maximum and the width corresponds to the difference between the two energies, where the amplitude squared is half of the maximum value. (In this case, the box amplitudes corresponding to decays into two pseudoscalars are included). The two entries under "real axis" are obtained with different Λ_b as explained in the main text.

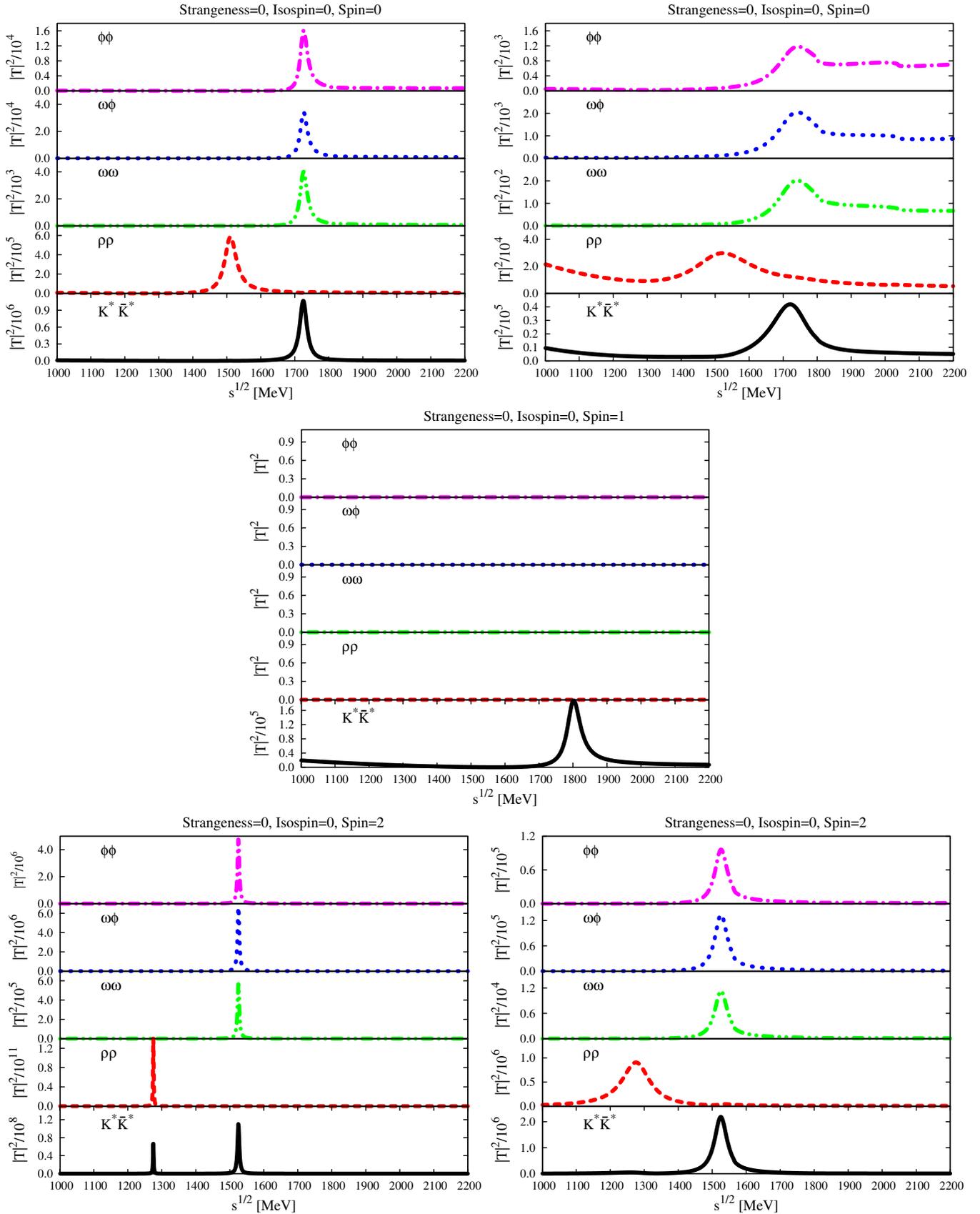| $I^G(J^{PC})$	Theory			PDG data		
	Pole position	Real axis		Name	Mass	Width
		$\Lambda_b = 1.4$ GeV	$\Lambda_b = 1.5$ GeV			
$0^+(0^{++})$	$(1512, 51)$	$(1523, 257)$	$(1517, 396)$	$f_0(1370)$	$1200 \sim 1500$	$200 \sim 500$
$0^+(0^{++})$	$(1726, 28)$	$(1721, 133)$	$(1717, 151)$	$f_0(1710)$	1724 ± 7	137 ± 8
$0^-(1^{+-})$	$(1802, 78)$	$(1802, 49)$		h_1		
$0^+(2^{++})$	$(1275, 2)$	$(1276, 97)$	$(1275, 111)$	$f_2(1270)$	1275.1 ± 1.2	$185.0^{+2.9}_{-2.4}$
$0^+(2^{++})$	$(1525, 6)$	$(1525, 45)$	$(1525, 51)$	$f_2'(1525)$	1525 ± 5	73^{+6}_{-5}
$1^-(0^{++})$	$(1780, 133)$	$(1777, 148)$	$(1777, 172)$	a_0		
$1^+(1^{+-})$	$(1679, 235)$	$(1703, 188)$		b_1		
$1^-(2^{++})$	$(1569, 32)$	$(1567, 47)$	$(1566, 51)$	$a_2(1700)??$		
$1/2(0^+)$	$(1643, 47)$	$(1639, 139)$	$(1637, 162)$	K_0^*		
$1/2(1^+)$	$(1737, 165)$	$(1743, 126)$		$K_1(1650)?$		
$1/2(2^+)$	$(1431, 1)$	$(1431, 56)$	$(1431, 63)$	$K_2^*(1430)$	1429 ± 1.4	104 ± 4

FIG. 4 (color online). $|T|^2$ in $(s, I) = (0, 0)$ for different spin channels without (left panel) and with the contributions of the box diagrams (right panel).

1. Spin $= 0$*;* $0^+(0^{++})$

Two poles are found in this channel: one at $(1512, -i26)$ MeV and another at $(1726, -i14)$ MeV, which we associate to the states $f_0(1370)$ and $f_0(1710)$ for the reasons given below. The couplings of these two states to the different coupled channels indicate that the $f_0(1370)$ is mainly a $\rho\rho$ state, while the $f_0(1710)$ is mainly a $K^*\bar{K}^*$ state.

From the plots with the contributions of the box diagrams, the peak positions and the widths are estimated to be $(1523, 257)$ MeV and $(1721, 133)$ MeV with the numbers in the parenthesis being (mass, width), respectively.

The relevant information from the PDG [38] is summarized in the following:

(i) The $f_0(1370)$ has a mass of $1200 \sim 1500$ MeV and a width of $200 \sim 500$ MeV. The debate about its mass continues nowadays; while a recent analysis advocates a mass around 1370 MeV [43], preliminary results from the Belle Collaboration rather point to a value around 1470 MeV [44]. Among its decay modes, according to the PDG [38], the 4π mode is larger than 72%, where the $\rho\rho$ mode is dominant. In our approach, the $\pi\pi$ mode is dominant, as can be seen from Table IV, which is consistent with the results of Ref. [45] and the recent analysis of D. V. Bugg [43].

(ii) The $f_0(1710)$ has a mass of 1724 ± 7 MeV and a width of $\Gamma = 137 \pm 8$ MeV. The main decay channel is through $K\bar{K}$, $\eta\eta$, and $\pi\pi$. The decay mode to $\omega\omega$ has been seen. This is in agreement with our findings since the two pseudoscalar box diagrams contain these decay channels. Indeed, we find that the $K\bar{K}$ decay channel is dominant. More specifically, our calculated branching ratios are $\sim 55\%$ for $K\bar{K}$, $\sim 27\%$ for $\eta\eta$, $< 1\%$ for $\pi\pi$, and $\sim 18\%$ for the vector-vector component. On the other hand, the PDG gives the following averages: $\Gamma(\pi\pi)/\Gamma(K\bar{K}) = 0.41^{+0.11}_{-0.17}$ and $\Gamma(\eta\eta)/\Gamma(K\bar{K}) = 0.48 \pm 0.15$ [38]. Our calculated branching ratio for the $\eta\eta$ channel is in agreement with their average, while the ratio for the $\pi\pi$ channel is much smaller. However, we notice that the above PDG $\Gamma(\pi\pi)/\Gamma(K\bar{K})$ ratio is taken from the BES experiment $J/\psi \to \gamma\pi^+\pi^-$ [46], which comes from a partial wave analysis that includes seven resonances. On the other hand, there is another BES experiment $J/\psi \to \omega K^+ K^-$ [47], which filters $I = 0$ automatically and gives an upper limit $\Gamma(\pi\pi)/\Gamma(K\bar{K}) < 11\%$ at the 95% confidence level. Clearly more analysis is advised to settle the issue.

(iii) We see that the $f_0(1370)$ is mainly $\rho\rho$, and the $f_0(1710)$ is mostly $K^*\bar{K}^*$. Although our picture for the resonances would correspond, in terms of quark degrees of freedom, to a four quark ($qq\bar{q}\bar{q}$) system, it is anyway interesting to recall that pictures for

these resonances in terms of $q\bar{q}$ also advocate ud components for the $f_0(1370)$ and strange quark components for the $f_0(1710)$ [38].

The $f_0(1500)$, on the hand, has a mass of 1505 ± 6 MeV and a width of $\Gamma = 109 \pm 7$ MeV. The width of the $f_0(1500)$ is too small to be associated to the lower scalar state that we get dynamically generated in the unitary approach, with a width of about 260 MeV.

2. Spin $= 1$*;* $0^-(1^{+-})$

One pole at $(1802, -i39)$ MeV is found. However, this state cannot be clearly identified with any of the h_1 states listed in the PDG. Note that this state is built only from $K^*\bar{K}^*$. The fact that this state couples only to $K^*\bar{K}^*$ and not to two pseudoscalars, as we discussed for the spin $= 1$ states, makes its observation difficult. However, the prediction is neat; $|T|^2$ is sizable compared to other resonances, and we find a clear pole on the complex plane associated to this resonance. On the other hand, the energy is such that it is slightly above the $K^*\bar{K}^*$ threshold. This fact, in addition to the width of the K^*, would make the observation of this state possible by looking at the $K\bar{K}\pi\pi$ decay channel, and even the $K\pi$ resonant shape could be partly reconstructed to give support to the $K^*\bar{K}^*$ nature of this resonance.

3. Spin $= 2$*;* $0^+(2^{++})$

Two poles are found on the complex plane: one at $(1275, -i1)$ MeV and the other at $(1525, -i3)$ MeV, which we associate to the $f_2(1270)$ and the $f_2'(1525)$. The lower one mainly couples to $\rho\rho$ and very weakly to $K^*\bar{K}^*$. This can be seen in the strengths of $|T|^2$ in the lower right-most panel of Fig. 4, and more clearly in the value of g for the couplings to the channels as shown in Table I. The higher resonance couples mainly to $K^*\bar{K}^*$, $\omega\phi$, and $\phi\phi$. As mentioned above, the masses of these two states have been used to fine-tune our subtraction constants.

From $|T|^2$ on the real axis obtained including box diagrams, one obtains the masses and widths as $(1276, 97)$ MeV and $(1525, 45)$ MeV. It is gratifying to see that the estimated widths are smaller than their experimental counterparts [$185.0^{+2.9}_{-2.4}$ MeV for the $f_2(1270)$ and 73^{+6}_{-5} MeV for the $f_2'(1525)$]. This should always be the case since other coupled channels, which we have not included, may also contribute. However, note that the order of magnitude is consistent and furthermore we predict a bigger width for the $f_2(1270)$ than for the $f_2'(1525)$ in spite of the fact that the higher mass resonance has more phase space to decay. We also see in Table IV that these widths get a bit bigger by increasing moderately the value of the Λ_b parameter of the form factors of Eqs. (26) and (27).

Once again it is interesting to compare the partial decay widths. For the $f_2(1270)$ we get most of the width from $\pi\pi$ decay. In the PDG, the branching ratios are 84.8% for $\pi\pi$,

4.6% for KK, and $<1\%$ for $\eta\eta$ [38], to be compared with our calculated numbers $\sim 88\%$ for $\pi\pi$, $\sim 10\%$ for $K\bar{K}$ and $<1\%$ for $\eta\eta$.

The case of the $f_2'(1525)$ is equally clarifying. We get most of the width from $K\bar{K}$ ($\sim 66\%$, compared to the branching ratio of 88.7% in the PDG [38]). Our calculated ratios are $\sim 21\%$ for $\eta\eta$, $\sim 1\%$ for $\pi\pi$, and $\sim 13\%$ for vector-vector component, while the PDG gives 10.4% for $\eta\eta$ and 0.8% for $\pi\pi$ [38]. The agreement is reasonable.

The position of the higher state at 1525 MeV is also close to the $f_2(1430)$ and the $f_2(1565)$. The $f_2(1430)$ is a little further away while the $f_2(1565)$ has a strong coupling to $\rho\rho$ decay mode, while in our calculation this state couples very weakly to the $\rho\rho$ channel; therefore, we do not favor the assignment to any of these two resonances.

B. Strangeness $= 0$ and Isospin $= 1$

In Fig. 5, we plot $|T_{ii}|$'s for the strangeness $= 0$ and isospin $= 1$ channel. Three resonances are found dynamically generated.

1. Spin $= 0$; $1^-(0^{++})$

One pole is found at $(1780, -i66)$ MeV, and it has the quantum numbers of a_0. It couples mostly to the $K^*\bar{K}^*$ channel. No a_0 around this energy region has been reported, according to the PDG [38].

Including the box diagrams, one gets $(1777, 148)$ MeV. It is seen that the inclusion of the box diagrams does not change much both the mass and the width of this state, meaning that it has a small branching ratio to two pseudoscalars.

This resonance can in principle be formed in $J/\psi \rightarrow \gamma K^*\bar{K}^*$ and $J/\psi \rightarrow \gamma K\bar{K}$. It is below the $K^*\bar{K}^*$ threshold and wider than the $0^-(1^{+-})$ state, and it could produce a broader bump close to the $K^*\bar{K}^*$ threshold. Such a feature does seem to show up in the BES experiment [48], but once again a new look at these data would be worthwhile.

2. Spin $= 1$; $1^+(1^{+-})$

This channel has the quantum numbers of b_1. One pole is found at $(1679, -i118)$ MeV, and it couples strongly to the $\rho\rho$ channel. Experimentally, no b_1 has been reported around this energy region.

This state does not decay into $\pi\pi$ but there should be no problem in studying the $\rho\rho$ invariant mass since the mass of the particle appears above the $\rho\rho$ threshold. Although several experiments have looked into $J/\psi \rightarrow 2(\pi^+\pi^-)\pi^0$ [49–52], none of them has looked at the $\rho\rho$ invariant mass distribution. We can only encourage further search in this direction once the previous works have proved the viability of the experiment.

3. Spin $= 2$; $1^-(2^{++})$

One pole is found at $(1569, -i16)$ MeV, and it couples strongly to $K^*\bar{K}^*$. Including the box diagrams, one obtains $(1567, 47)$ MeV. The closest a_2 in energy included in the PDG is the $a_2(1700)$ with a mass of 1732 ± 16 MeV and a width of 194 ± 40 MeV, whose decay to $\omega\rho$ has been seen [38]. It should be noted that the properties of this particle are not well determined. Different experiments report quite different values for both its mass and width [38].

In order to see if the resonance we get could be associated to the $a_2(1700)$, we have changed the values of the subtraction constants to move its pole position to larger mass values. For instance, if we change the value of $a_{K^*\bar{K}^*}$ from -1.726 [determined by the $f_2'(1525)$ mass] to -1.0, we would have a mass of 1704 MeV and a width of 49 MeV. The mass would be much closer to the PDG average but the width would still be much smaller. A modification of the values of the subtraction constants of the other two coupled channels ($\rho\omega$ and $\rho\phi$) leads to similar conclusions. Given the large uncertainty in the experimental status of the $a_2(1700)$, we find no particular reason to associate the state we generate dynamically to this resonance.

We also note that the modification of $a_{K^*\bar{K}^*}$ has small influences on the states with the quantum numbers of b_1 and a_0, which we studied in the two preceding subsections, and it does not allow us to associate these two states with any well-known resonances listed in the PDG.

C. strangeness $= 1$ and Isospin $= 1/2$

In Fig. 6, we plot $|T_{ii}|^2$'s for the strangeness $= 1$ and isospin $= 1/2$ channel.

1. Spin $= 0$; $1/2(0^+)$

One pole is found at $(1643, -i24)$ MeV, and it couples strongly to ρK^*. Including the box diagrams, one obtains $(1639, 139)$ MeV.

At first sight, this state might be the $K(1630)$. On the other hand, the $K(1630)$ $[1/2(?^?)]$, with a mass of 1629 ± 7 MeV and a width of 16^{+19}_{-16} MeV [38], might be too narrow to be associated with the state dynamically generated from vector-vector interaction. There is another indication not to associate the state we find with the $K(1630)$, since our main decay mode is πK from the two meson box diagrams, while the decay mode observed in the PDG is $K\pi^+\pi^-$.

2. Spin $= 1$; $1/2(1^+)$

One pole is found at $(1737, -i82)$ MeV, and it couples strongly to ρK^*. No K_1 around this energy region is reported in the PDG, with the closest one being the $K_1(1650)$ with a mass of 1650 ± 50 MeV and a width of 150 ± 50 MeV [38]. The width of the $K_1(1650)$ is
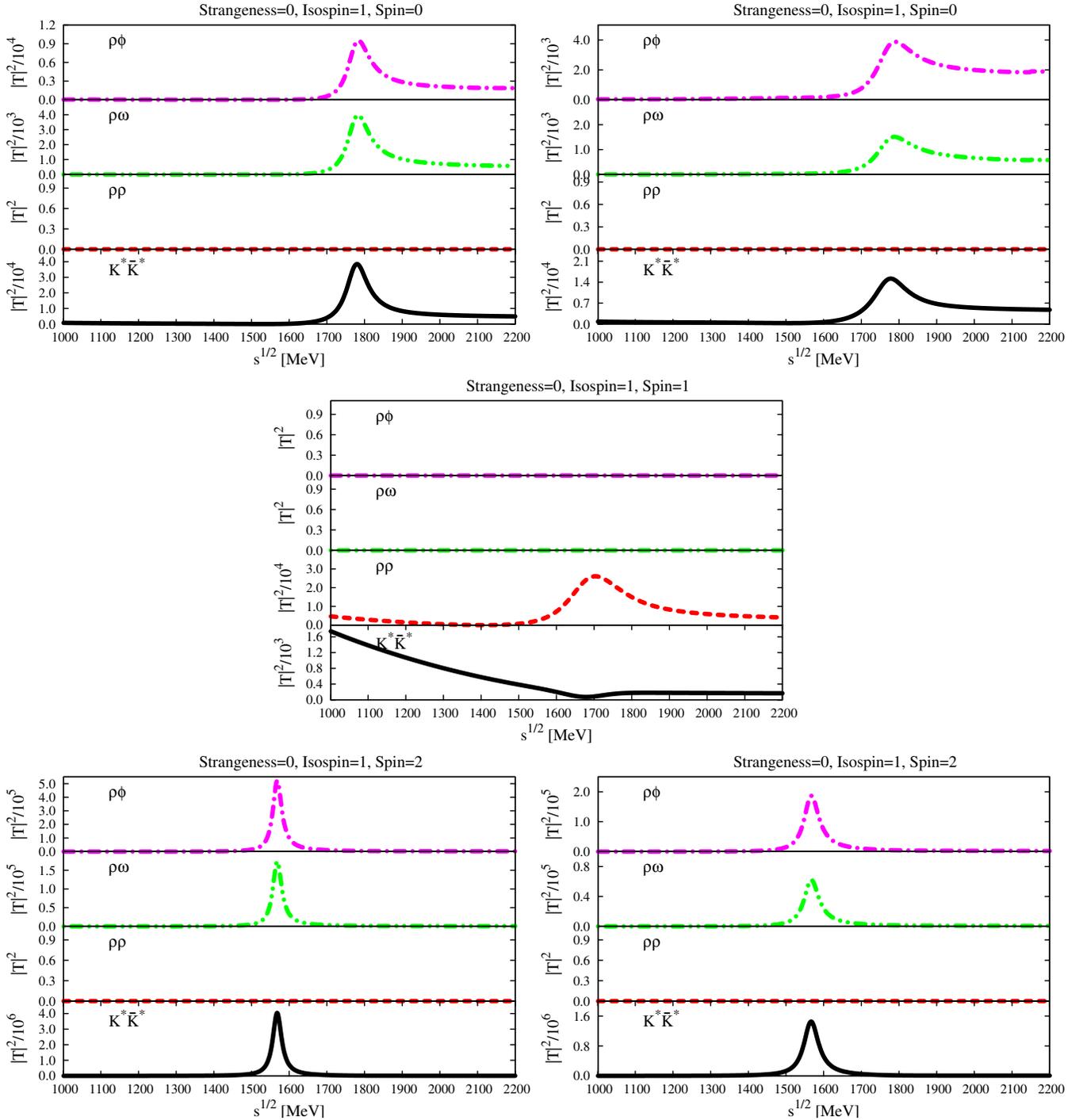
FIG. 5 (color online).   The same as Fig. 4, but for the $(s, I) = (0, 1)$ channel.

150 MeV, and we also obtain a width of about 160 MeV. Since the width is twice as large as the difference of masses the association of these two states is tempting. There is another feature that could support this association; in spite of the limited information on this resonance, the only decay channels observed are $K\pi\pi$, $K\phi$, but none on two pseudoscalars for which there is more phase space. This is in agreement with the fact that our state of spin 1 does not decay into two pseudoscalars, as we have mentioned.

3. Spin = 2; $1/2(2^+)$

One pole is found at $(1431, -i1)$ MeV, which might correspond to the $K_2^*(1430)$, and its position has been used to fine-tune the subtraction constants in this channel. Including the box diagrams, one obtains $(1431, 56)$ MeV.

According to the PDG, the $K_2^*(1430)$ has a mass of 1429 ± 1.4 MeV and a width of 104 ± 4 MeV. Among its decays modes, the $K^*\pi\pi$ mode amounts to $(13.4 \pm 2.2)\%$,
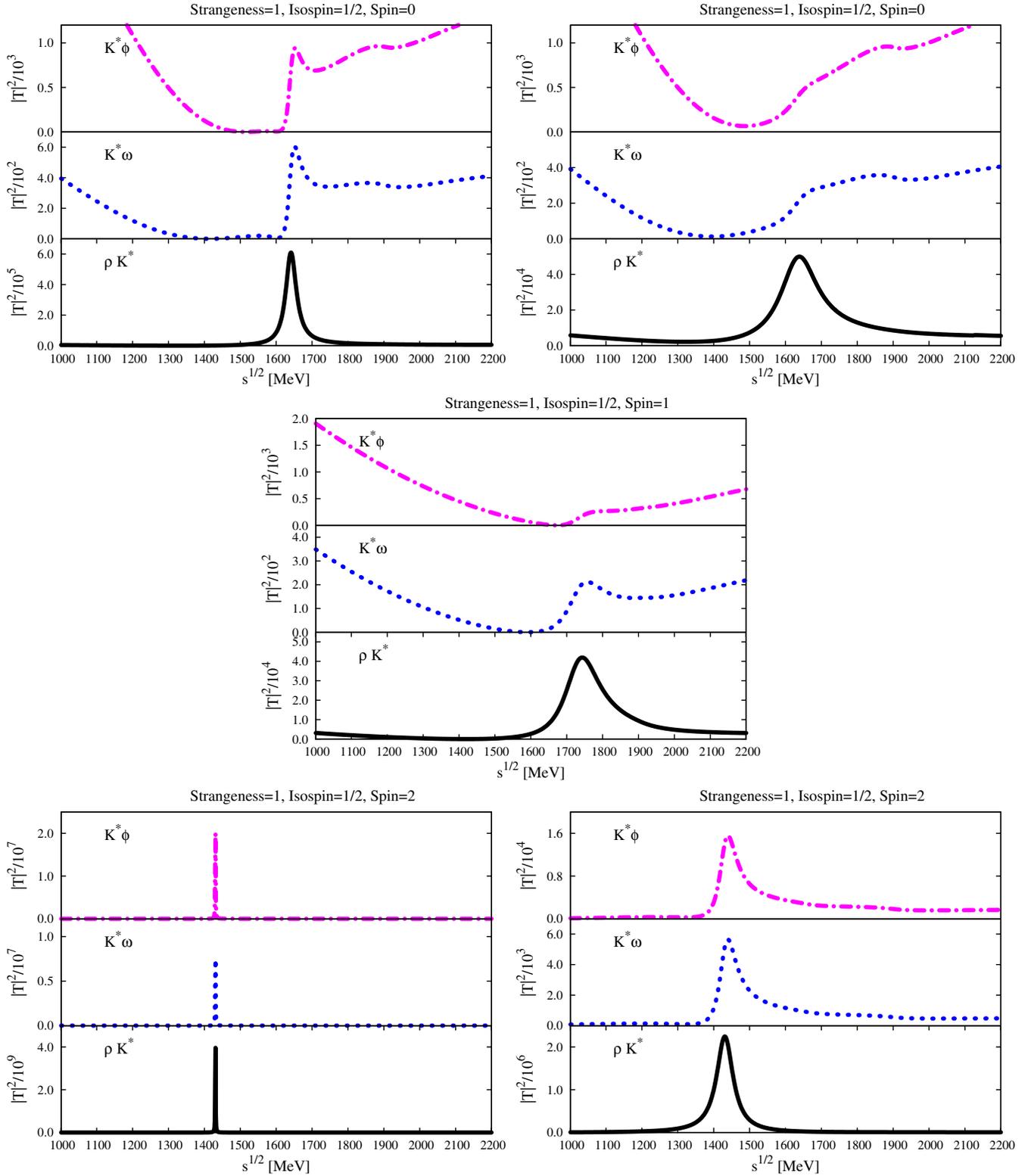
FIG. 6 (color online).   The same as Fig. 4, but for the $(s, I) = (1, 1/2)$ channel.

some of which might be ρK^*; the $K\pi$ mode amounts to $(49.9 \pm 1.2)\%$. Therefore, the width that we obtain is in reasonable agreement with the data.

D. Other channels

It is interesting to note that out of the 21 combinations of strangeness, isospin and spin, we have found resonances only in nine of them. In all the "exotic" channels, from the point of view that they cannot be formed from $q\bar{q}$ states, we did not find dynamically generated resonances, including the three strangeness $= 0$, isospin $= 2$ channels, the three strangeness $= 1$, isospin $= 3/2$ channels, the six strangeness $= 2$ channels (with either isospin $= 0$ or isospin $= 1$).

It is also interesting to note that although no poles are found on the complex plane, there do exist some structures on the real axis. For instance, in the (strangeness $= 0$, isospin $= 2$) channel, one finds a dip around $\sqrt{s} = 1300$ MeV in the spin $= 0$ channel, and a broad bump in the spin $= 2$ channel around $\sqrt{s} = 1400$ MeV, as can be clearly seen from Fig. 7. In the (strangeness $= 1$, isospin $=$

$3/2$) and (strangeness $= 2$, isospin $= 1$) channels, one observes similar structures occurring at shifted energies due to the different masses of the ρ and the K^*, as can be seen from Figs. 8 and 10.

It is worthwhile mentioning that we obtain some broad bumps in the following four channels: (strangeness $= 0$, isospin $= 2$, spin $= 2$), (strangeness $= 1$, isospin $= 3/2$, spin $= 2$), (strangeness $= 2$, isospin $= 0$, spin $= 1$), and (strangeness $= 2$, isospin $= 1$, spin $= 2$), see Figs. 7–10. All of these are exotic channels. As mentioned before, none of the broad peaks corresponds to a pole on the complex plane, and hence, according to the common criteria, they do not qualify as resonances. Let us see what is the experimental information in these sectors. In the PDG [38], we find the $X(1600)$ with strangeness $= 0$ and quantum numbers $2^+(2^{++})$ with a mass of 1600 ± 100 MeV and a width of 400 ± 200 MeV. There are candidates in theoretical models for this. Indeed, based on a theoretical estimate of the twist 4 contributions in explaining the recent L3 data on $\gamma^*\gamma \to \rho^0\rho^0$ and $\gamma^*\gamma \to \rho^+\rho^-$ [53,54], I. V. Anikin *et al.* advocate the existence of an
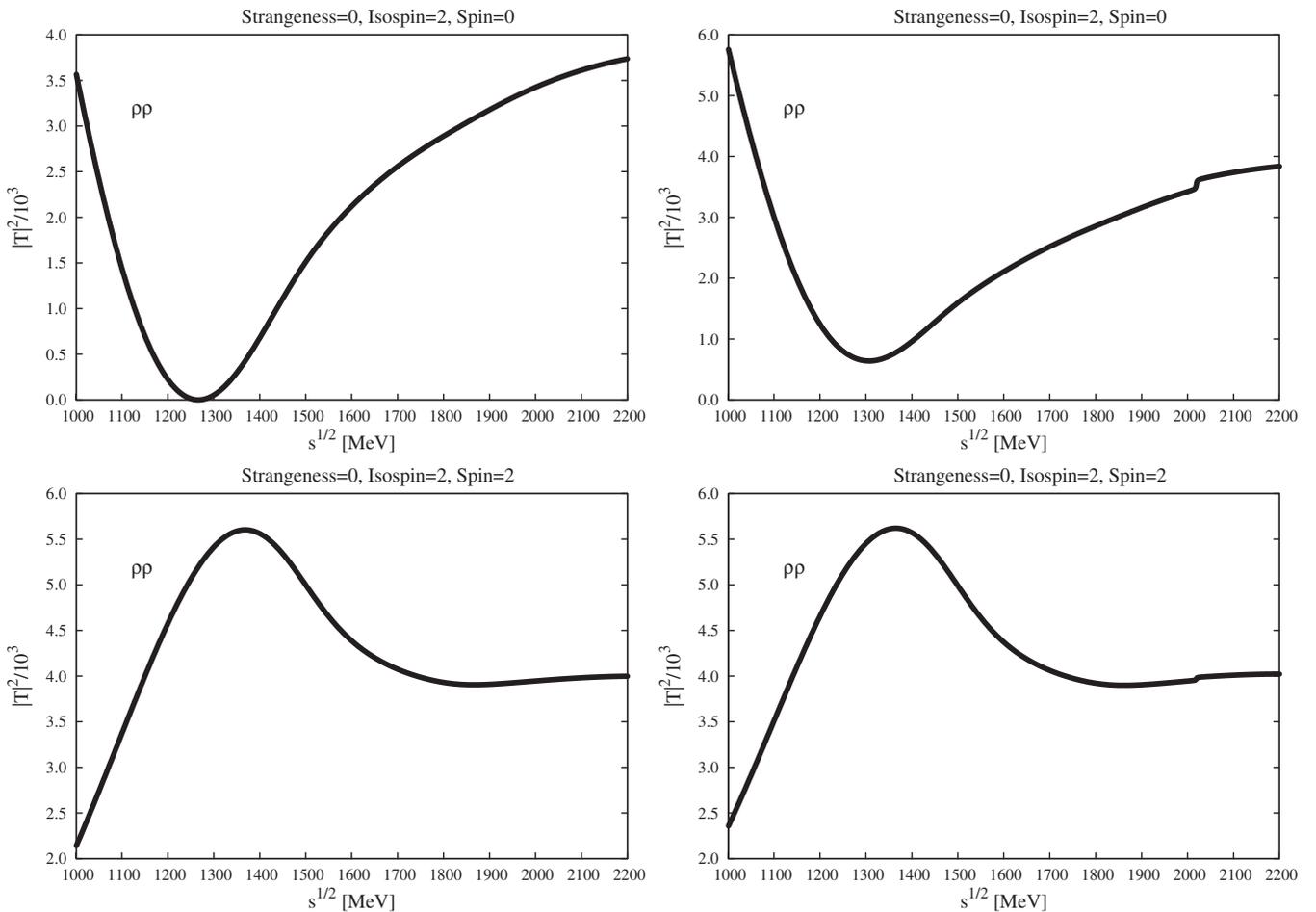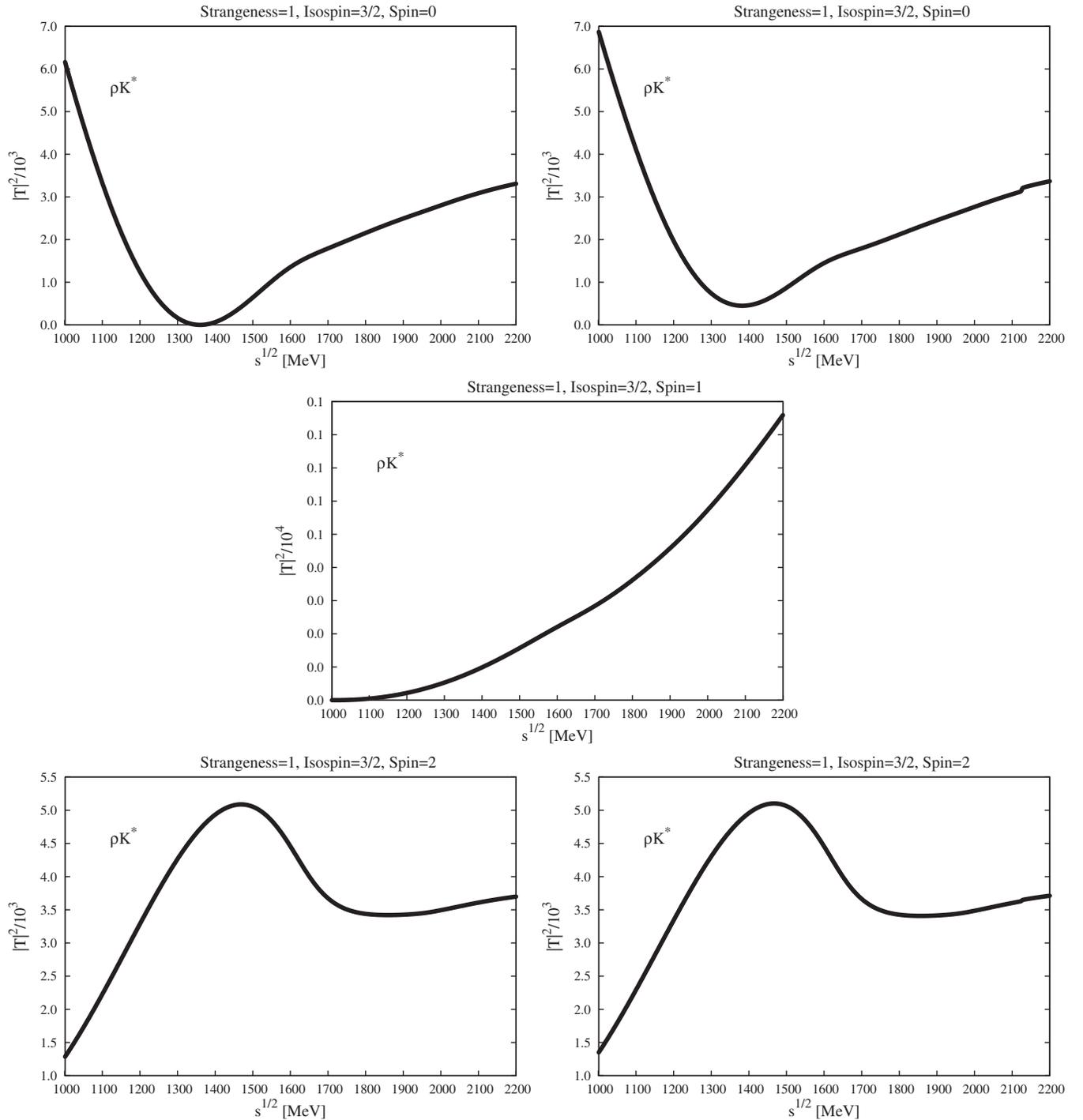

FIG. 7. The same as Fig. 4, but for the $(s, I) = (0, 2)$ channel. Note that we have not shown the results for spin $= 1$ channel, since there are no interactions here because of the properties of identical particles.

FIG. 8.   The same as Fig. 4, but for the $(s, I) = (1, 3/2)$ channel.

exotic isotensor resonance with a mass of ~ 1.5 GeV and a width of ~ 0.4 GeV [55]. However, we can offer here a different interpretation for the experimental bump, since it might be identified with the broad bump that we get with these quantum numbers around 1400 MeV and a similar width. Indeed, the experiment where the bump is reported [56] sees it in the $\rho^0 \rho^0$ channel. It looks rather clear that

the bump observed is the one we find in the $\rho \rho$ amplitude, and this does not qualify as a resonance.

One can also speculate about the scalar $2^+(0^{++})$ state reported in the PDG around 1400 MeV from a weak signal found as a broad bump in Ref. [57]. As can be seen from the upper panel of Fig. 7, we find a dip in $\rho \rho$ amplitude squared in this channel around 1300 MeV. Such a dip in the
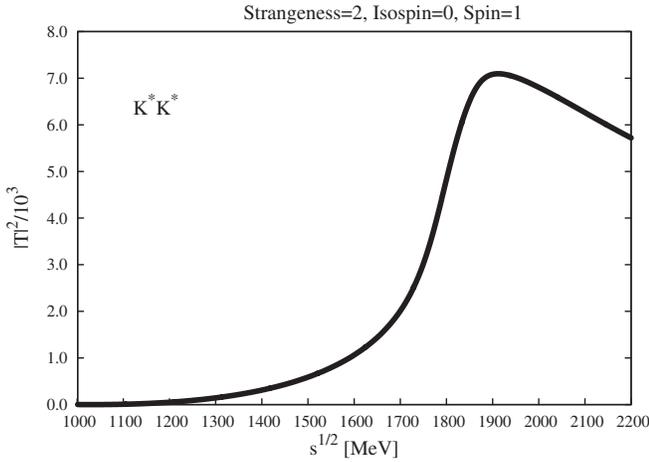
FIG. 9. The same as Fig. 4, but for the $(s, I) = (2, 0)$ channel. There are no interactions in spin = 0 and spin = 2 channels due to the properties of identical particles.

$\rho\rho$ amplitude can lead to a bump in $\pi^+\pi^+$ production, in an analogous way as what occurs to the $f_0(980)$ resonance, which shows up as a dip in the $\pi\pi$ cross section but as a peak in $\gamma\gamma$ or other production processes [58]. Once again, the bump could not be associated to a pole in our approach and, hence, would not qualify as a resonance.

We do not find any candidate in the PDG to our broad bumps in the strange sector. However, the findings of the present work should be kept in mind in the verge of possible claims for exotic strange mesons from bumps observed in cross sections.

We would like to give some perspective to the results obtained here. We have used as building blocks for our states only vector mesons. Two pseudoscalar states have been considered for the decay but not incorporated as coupled channels. Other possible channels, like $\sigma\sigma$ in the case of $\rho\rho$ scattering, are also omitted in our approach. The contributions of these channels in a coupled channel approach would be advisable should one try to get, for instance, $\pi\pi$ scattering in a broad range of energies. Such an approach has been undertaken in Ref. [45].[1] However,
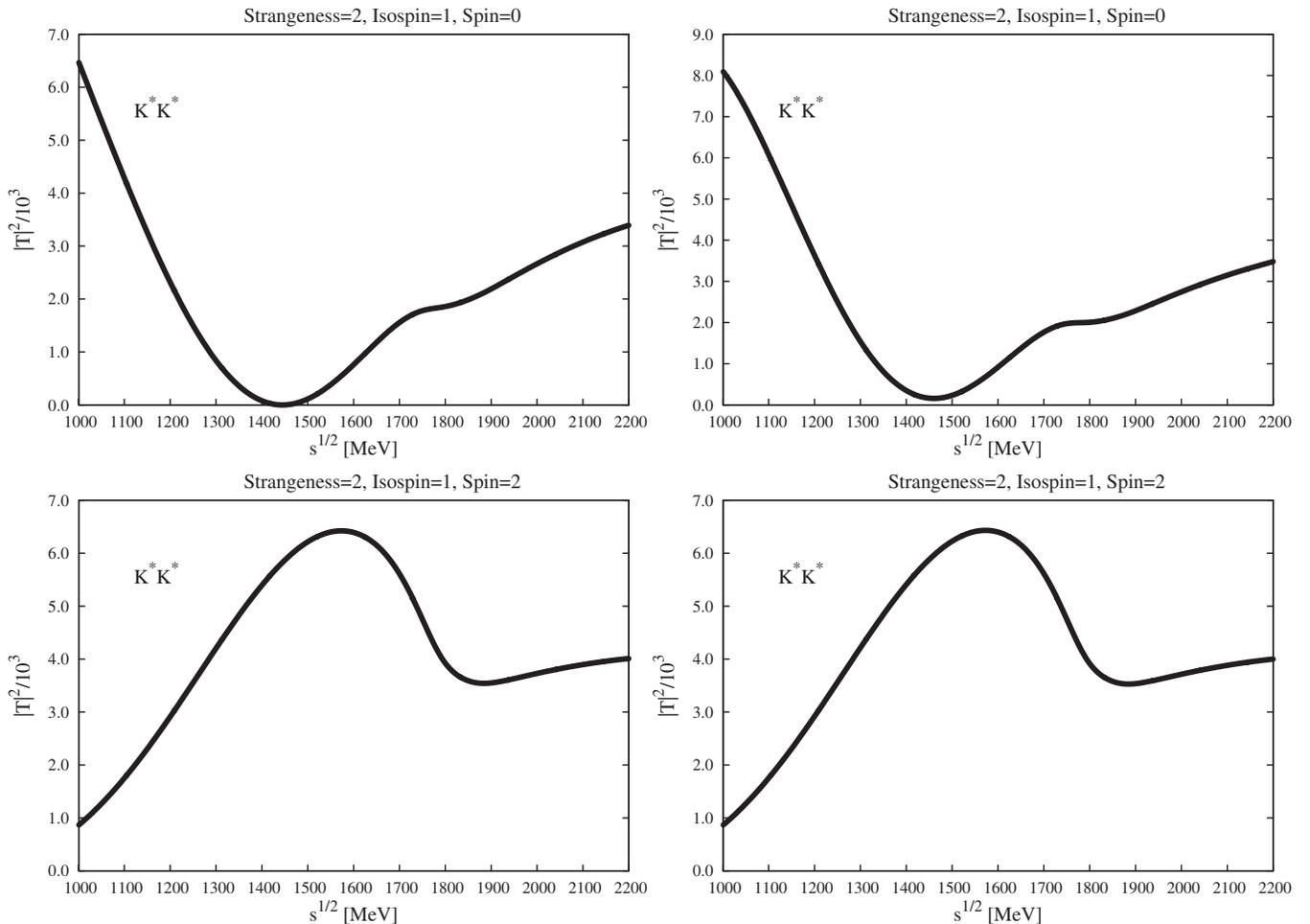

FIG. 10. The same as Fig. 4, but for the $(s, I) = (2, 1)$ channel. There are no interactions in spin = 1 channel due to the properties of identical particles.

this is not our purpose here. We take only vector mesons as building blocks with their respective interactions, and we look at the states that are generated dynamically from these interactions. We then get a few meson resonances, but not all. This tells us which resonances are most likely to be essentially vector-vector "molecules," and this is the purpose of the present work.

IV. SUMMARY AND CONCLUSIONS

We have performed a study of vector meson-vector meson interaction using a unitary approach. Employing the coupled channel Bethe-Salpeter equation to unitarize the tree-level transition amplitudes obtained from the hidden-gauge Lagrangians, 11 states in nine strangeness-isospin-spin channels were dynamically generated. Among them, five states are associated to those reported in the PDG, i.e., the $f_0(1370)$, the $f_0(1710)$, the $f_2(1270)$, the $f_2'(1525)$, the $K_2^*(1430)$. The association of two other states, the $a_2(1700)$ and the $K_1(1650)$, are likely, particularly the $K_1(1650)$, but less certain. The $f_0(1370)$ and $f_2(1270)$ have already been reported in Ref. [35], and they are built mainly from the $\rho\rho$ interaction. We reconfirm the findings of this early work after including all SU(3) coupled channels. The box diagrams in our approach provide a mechanism for the dynamically generated states to decay into two pseudoscalars. This mechanism broadens the scalar states and the tensor states in the strangeness $= 0$ and isospin $= 0$ channel and the strangeness $= 1$ and isospin $= 1/2$ channel but not for the spin $= 1$ states. On the other hand, this mechanism contributes little to the widths of the scalar and tensor states in the strangeness $= 0$ and isospin $= 1$ channel.

We have used the masses of the $f_2(1270)$, the $f_2'(1525)$, and the $K_2^*(1430)$ to fine-tune the free parameters of the approach, the subtraction constants in the vector-vector loop functions. After this is done, there is little freedom in changing the total decay widths and practically no freedom in changing the decay branching ratios. It is then gratifying to see that the total and partial decay widths of these resonances are consistent with the data. It is also interesting to see that the two f_0 states appear at proper positions with reasonable widths compared to the data.

Four of the 11 dynamically generated states can not be associated with known states in the PDG. These states either have small branching ratios into two pseudoscalars or are in the strangeness $= 1$ sector, where the experimental situation is less satisfactory than in the strangeness $= 0$ sector.

Another interesting finding of our work was the broad bumps found in four exotic channels, none of which corresponded to poles on the complex plane. One of these

---

[1]This work is now being extended and we do not elaborate further on it, but one should keep track of new developments along this line [59].

bumps was identified with the structure of the $X(1600)$, which is reported in the PDG as a resonant state with $2^+(2^{++})$. Our study provides an interpretation of this bump, stemming from the $\rho\rho$ interaction in this channel, which, however, does not have any pole associated and, hence, does not qualify as a resonance.

For the resonances predicted and not reported in the PDG we offered suggestions on how they could be searched experimentally with present experiment facilities, and we can only encourage further work in this direction.

APPENDIX A: TREE-LEVEL TRANSITION AMPLITUDES OF THE FOUR-VECTOR CONTACT DIAGRAMS AND OF THE $t(u)$-CHANNEL VECTOR-EXCHANGE DIAGRAMS

We show here in Tables V and VI the amplitudes for only the strangeness $= 0$, isospin $= 0$, and spin $= 0$ channel to save space. The rest of the amplitudes for all the other channels can be found in the appendix of Ref. [40] (the arXiv version of the present paper).

APPENDIX B: BOX DIAGRAM AMPLITUDES

In this section, we provide the explicit box diagram amplitudes, corresponding to Eq. (22), for different strangeness and isospin but only spin $= 0$ channels. Those amplitudes for spin $= 2$ channels can be obtained by multiplying $2/5$ to the corresponding spin $= 0$ amplitudes, as explained in the main text. To simplify the expressions, we have used the abbreviations defined in Table VII.

(1) Strangeness $= 0$, isospin $= 0$, and spin $= 0$: There are five channels, i.e., $K^*\bar{K}^*$, $\rho\rho$, $\omega\omega$, $\omega\phi$, $\phi\phi$, with the order of 1, 2, 3, 4, 5:

TABLE V. The V_{ij}'s of the four-vector contact term in the strangeness $= 0$, isospin $= 0$ and spin $= 0$ channel.

	$K^*\bar{K}^*$	$\rho\rho$	$\omega\omega$	$\omega\phi$	$\phi\phi$
$K^*\bar{K}^*$	$6g^2$	$2\sqrt{3}g^2$	$-2g^2$	$4g^2$	$-4g^2$
$\rho\rho$		$8g^2$	0	0	0
$\omega\omega$			0	0	0
$\omega\phi$				0	0
$\phi\phi$					0

TABLE VI. The V_{ij}'s for the $t(u)$-channel vector-exchange diagrams in the strangeness $= 0$, isospin $= 0$ and spin $= 0(2)$ channel.

	$K^*\bar{K}^*$	$\rho\rho$	$\omega\omega$	$\omega\phi$	$\phi\phi$
$K^*\bar{K}^*$	$\frac{g^2(M_\rho^2 M_\phi^2 + (2M_\rho^2 + 3M_\phi^2)M_\omega^2)(4M_{K^*}^2 - 3s)}{4M_\rho^2 M_\phi^2 M_\omega^2}$	$\frac{\sqrt{3}g^2(2M_\rho^2 + 2M_{K^*}^2 - 3s)}{2M_{K^*}^2}$	$-\frac{g^2(2M_\omega^2 + 2M_{K^*}^2 - 3s)}{2M_{K^*}^2}$	$\frac{g^2(M_\phi^2 + M_\omega^2 + 2M_{K^*}^2 - 3s)}{M_{K^*}^2}$	$\frac{g^2(-2M_\phi^2 - 2M_{K^*}^2 + 3s)}{M_{K^*}^2}$
$\rho\rho$		$2g^2(4 - \frac{3s}{M_\rho^2})$	0	0	0
$\omega\omega$			0	0	0
$\omega\phi$				0	0
$\phi\phi$					0

$$v_{1,1} = 60g^4(3\tilde{G}_1 + 3\tilde{G}_2 + 12\tilde{G}_3 + 4\tilde{G}_4 + 3\tilde{G}_5 + 3\tilde{G}_6),$$

$$v_{1,2} = 40\sqrt{3}g^4(3\tilde{G}_7 + 8\tilde{G}_8 + 3\tilde{G}_9),$$

$$v_{1,3} = -120g^4(\tilde{G}_7 + \tilde{G}_9),$$

$$v_{1,4} = 120g^4(\tilde{G}_7 + \tilde{G}_7(u) + \tilde{G}_9 + \tilde{G}_9(u)),$$

$$v_{1,5} = -240g^4(\tilde{G}_7 + \tilde{G}_9),$$

$$v_{2,2} = 80g^4(3\tilde{G}_{10} + 16\tilde{G}_{11}),$$

$$v_{2,3} = -80\sqrt{3}g^4\tilde{G}_{10},$$

$$v_{2,4} = 80\sqrt{3}g^4(\tilde{G}_{10} + \tilde{G}_{10}(u)),$$

$$v_{2,5} = -160\sqrt{3}g^4\tilde{G}_{10}, \quad v_{3,3} = 80g^4\tilde{G}_{10},$$

$$v_{3,4} = -80g^4(\tilde{G}_{10} + \tilde{G}_{10}(u)), \quad v_{3,5} = 160g^4\tilde{G}_{10},$$

$$v_{4,4} = 160g^4(\tilde{G}_{10} + \tilde{G}_{10}(u)), \quad v_{4,5} = -320g^4\tilde{G}_{10},$$

$$v_{5,5} = 320g^4\tilde{G}_{10}.$$

(2) Strangeness $= 0$, isospin $= 1$, and spin $= 0$: There are four channels, i.e., $K^*\bar{K}^*$, $\rho\rho$, $\rho\omega$, $\rho\phi$, with the order 1, 2, 3, 4:

TABLE VII. The abbreviations used in calculating the box diagrams: $\tilde{G}_i = G_4(m_{p1}, m_{p2}, m_{p3}, m_{p4}, s, k_1^0, k_2^0, k_3^0, k_4^0)$ with $i = 1 \cdots 20$ and $p1$, $p2$, $p3$, $p4$ the particles appearing in the box diagram with the order as given in Fig. 2. In the text, $\tilde{G}_i(u) = G_4(m_{p1}, m_{p2}, m_{p3}, m_{p4}, s, k_1^0, k_2^0, k_4^0, k_3^0)$.

i	$p1$	$p2$	$p3$	$p4$	i	$p1$	$p2$	$p3$	$p4$
1	η	K	η	K	2	η	K	π	K
3	K	η	K	η	4	K	π	K	π
5	π	K	η	K	6	π	K	π	K
7	η	K	K	K	8	K	π	π	π
9	π	K	K	K	10	K	K	K	K
11	π	π	π	π	12	K	η	K	π
13	K	π	K	η	14	K	K	K	η
15	K	K	K	π	16	K	K	π	π
17	π	π	K	K	18	π	π	π	K
19	K	η	K	K	20	K	π	K	K

$$v_{1,1} = 20g^4(9\tilde{G}_1 - 3\tilde{G}_2 + 12\tilde{G}_{12} + 12\tilde{G}_{13}$$
$$- 3\tilde{G}_5 + \tilde{G}_6),$$

$$v_{1,2} = 0,$$

$$v_{13} = -20\sqrt{2}g^4(3\tilde{G}_7 + 3\tilde{G}_7(u) - \tilde{G}_9 - \tilde{G}_9(u)),$$

$$v_{1,4} = 40g^4(3\tilde{G}_7 + 3\tilde{G}_7(u) - \tilde{G}_9 - \tilde{G}_9(u)),$$

$$v_{2,2} = v_{2,3} = v_{2,4} = 0,$$

$$v_{3,3} = 80g^4(\tilde{G}_{10} + \tilde{G}_{10}(u))),$$

$$v_{3,4} = -80\sqrt{2}g^4(\tilde{G}_{10} + \tilde{G}_{10}(u)),$$

$$v_{4,4} = 160g^4(\tilde{G}_{10} + \tilde{G}_{10}(u)).$$

(3) Strangeness $= 0$, isospin $= 2$, and spin $= 0$: There is only one channel in this sector, i.e., $\rho\rho$:

$$v = 320g^4\tilde{G}_{11}.$$

(4) Strangeness $= 1$, isospin $= 1/2$, and spin $= 0$: There are three channels, i.e., ρK^*, $K^*\omega$, and $K^*\phi$, with the order 1, 2, 3:

$$v_{1,1} = 20g^4(9\tilde{G}_{14} + \tilde{G}_{15} + 4\tilde{G}_{16}(u) + 4\tilde{G}_{17}(u)$$
$$+ 16\tilde{G}_{18}),$$

$$v_{1,2} = -20\sqrt{3}g^4(3\tilde{G}_{14}(u) - \tilde{G}_{15}(u) - 4\tilde{G}_{17}),$$

$$v_{1,3} = 20\sqrt{6}g^4(3\tilde{G}_{14}(u) - \tilde{G}_{15}(u) - 4\tilde{G}_{17}),$$

$$v_{2,2} = 60g^4(\tilde{G}_{19} + \tilde{G}_{20}),$$

$$v_{2,3} = -60\sqrt{2}g^4(\tilde{G}_{19} + \tilde{G}_{20}),$$

$$v_{3,3} = 120g^4(\tilde{G}_{19} + \tilde{G}_{20}).$$

(5) Strangeness $= 1$, isospin $= 1/2$, and spin $= 0$: There is only one channel in this sector, i.e., ρK^*:

$$v = 80g^4(\tilde{G}_{15} + \tilde{G}_{16}(u) + \tilde{G}_{17}(u) + \tilde{G}_{18}).$$

(6) Strangeness $= 2$, isospin $= 0$, and spin $= 0$: There is only one channel in this sector, i.e., K^*K^*:

$$v = 0.$$

(7) Strangeness $= 2$, isospin $= 1$, and spin $= 0$: There is only one channel in this sector, i.e., $K^* K^*$:

$$v = 20g^4(9\tilde{G}_1 + 3\tilde{G}_2 + 3\tilde{G}_5 + \tilde{G}_6).$$

APPENDIX C: G_n IN THE EVALUATION OF THE FOUR-POINT LOOP FUNCTION

Here we provide the explicit form of G_n, which appears in the evaluation of the four-point loop function G_4 [Eq. (28)]. The symbols are the same as in the main text, except here we have replaced k_1^0, k_2^0, k_3^0, and k_4^0 by E_1, E_2, E_3, and E_4.

$$
\begin{aligned}
G_n ={}& \omega_1(\omega_3(\omega_2 + \omega_4)E_3^2 - 2P^0\omega_3\omega_4 E_3 - (\omega_2 + \omega_3)((\omega_3 + \omega_4)\omega_2^2 + (\omega_3^2 + 3\omega_4\omega_3 + 2\omega_4^2)\omega_2 \\
&+ \omega_4((\omega_3 + \omega_4)^2 - s)))E_1^4 + 2\omega_1(-\omega_3(\omega_2 + \omega_4)E_3^3 + P^0\omega_3\omega_4 E_3^2 + \omega_3(\omega_2^3 + 2(\omega_3 + \omega_4)\omega_2^2 \\
&+ (\omega_3^2 + 4\omega_4\omega_3 + 2\omega_4^2)\omega_2 + \omega_4(s + (\omega_3 + \omega_4)^2))E_3 + P^0(\omega_2 + \omega_3)\omega_4(-s + \omega_2^2 + (\omega_3 + \omega_4)^2 \\
&+ \omega_2(\omega_3 + 2\omega_4)))E_1^3 + \omega_1(\omega_3(\omega_2 + \omega_4)E_3^4 + 2P^0\omega_3\omega_4 E_3^3 - 2\omega_3(\omega_2^3 + \omega_3\omega_2^2 + \omega_3(\omega_3 + 2\omega_4)\omega_2 \\
&+ \omega_1^2(\omega_2 + \omega_4) + \omega_1(\omega_2 + \omega_4)(\omega_2 + \omega_3 + \omega_4) + \omega_4(3s + \omega_3^2 + \omega_3\omega_4))E_3^2 \\
&+ 2P^0\omega_3\omega_4(s + 2\omega_1^2 - 2\omega_2^2 - \omega_3^2 - \omega_4^2 - 4\omega_2\omega_4 - 4\omega_3\omega_4 + 2\omega_1(\omega_2 + \omega_3 + \omega_4))E_3 \\
&+ (\omega_2 + \omega_3)((\omega_3 + \omega_4)\omega_2^4 + (\omega_3^2 + 3\omega_4\omega_3 + 2\omega_4^2)\omega_2^3 + (\omega_3^3 + 5\omega_4\omega_3^2 + 6\omega_4^2\omega_3 + 2\omega_4^3 - 2s\omega_4)\omega_2^2 \\
&+ (\omega_3^4 + 3\omega_4\omega_3^3 + 6\omega_4^2\omega_3^2 + 2\omega_4(s + 3\omega_4^2)\omega_3 + 2\omega_4^4 - 2s\omega_4^2)\omega_2 + \omega_4(s^2 - 2(\omega_3^2 + \omega_4\omega_3 + \omega_4^2)s \\
&+ (\omega_3 + \omega_4)^2(\omega_3^2 + \omega_4^2)) + 2\omega_1^2((\omega_3 + \omega_4)\omega_2^2 + (\omega_3^2 + 3\omega_4\omega_3 + 2\omega_4^2)\omega_2 + \omega_4((\omega_3 + \omega_4)^2 - s)) \\
&+ 2\omega_1(\omega_2 + \omega_3 + \omega_4)((\omega_3 + \omega_4)\omega_2^2 + (\omega_3^2 + 3\omega_4\omega_3 + 2\omega_4^2)\omega_2 + \omega_4((\omega_3 + \omega_4)^2 - s))))E_1^2 \\
&- 2\omega_1(P^0\omega_3\omega_4 E_3^4 - \omega_3(\omega_2^3 + 2\omega_4\omega_2^2 + 2\omega_4^2\omega_2 + \omega_4^3 + 2\omega_1(\omega_2 + \omega_4)^2 + s\omega_4 + \omega_1^2(\omega_2 + \omega_4))E_3^3 \\
&+ P^0\omega_3\omega_4(-s + \omega_1^2 + 2\omega_2^2 - 2\omega_3^2 + \omega_4^2 - 2\omega_2\omega_3 + 4\omega_2\omega_4 - 2\omega_3\omega_4 + \omega_1(4\omega_2 - 2\omega_3 + 4\omega_4))E_3^2 \\
&+ \omega_3(\omega_2^5 + 2(\omega_3 + \omega_4)\omega_2^4 + (\omega_3^2 + 4\omega_4\omega_3 + 2\omega_4^2)\omega_2^3 + 2\omega_4(s + (\omega_3 + \omega_4)^2)\omega_2^2 \\
&+ 2\omega_4((2\omega_3 - \omega_4)s + \omega_4(\omega_3 + \omega_4)^2)\omega_2 + \omega_4(s^2 + (\omega_3^2 - 2\omega_4\omega_3 - 2\omega_4^2)s + \omega_4^2(\omega_3 + \omega_4)^2) \\
&+ \omega_1^2(\omega_2^3 + 2(\omega_3 + \omega_4)\omega_2^2 + (\omega_3^2 + 4\omega_4\omega_3 + 2\omega_4^2)\omega_2 + \omega_4(s + (\omega_3 + \omega_4)^2)) \\
&+ 2\omega_1(\omega_2^4 + 2(\omega_3 + \omega_4)\omega_2^3 + (\omega_3^2 + 4\omega_4\omega_3 + 2\omega_4^2)\omega_2^2 + 2\omega_4(s + (\omega_3 + \omega_4)^2)\omega_2 \\
&+ \omega_4((2\omega_3 - \omega_4)s + \omega_4(\omega_3 + \omega_4)^2)))E_3 + P^0(\omega_2 + \omega_3)\omega_4(\omega_2^4 + \omega_3\omega_2^3 + 2\omega_4\omega_2^3 + \omega_3^2\omega_2^2 \\
&+ \omega_4^2\omega_2^2 + 2\omega_3\omega_4\omega_2^2 + \omega_3^3\omega_2 + \omega_3\omega_4^2\omega_2 + 2\omega_3^2\omega_4\omega_2 + \omega_3^4 + \omega_3^2\omega_4^2 - s(\omega_1^2 + 2(\omega_2 + \omega_3)\omega_1 + \omega_2^2 \\
&+ \omega_3^2 + \omega_2\omega_3) + 2\omega_3^3\omega_4 + \omega_1^2(\omega_2^2 + (\omega_3 + 2\omega_4)\omega_2 + (\omega_3 + \omega_4)^2) + 2\omega_1(\omega_2^3 + (\omega_3 + 2\omega_4)\omega_2^2 \\
&+ (\omega_3 + \omega_4)^2\omega_2 + \omega_3(\omega_3 + \omega_4)^2)))E_1 - (\omega_1 + \omega_2)(\omega_3((\omega_2 + \omega_4)\omega_1^2 + (\omega_2^2 + 3\omega_4\omega_2 + 2\omega_4^2)\omega_1 \\
&+ \omega_4((\omega_2 + \omega_4)^2 - s))E_3^4 + 2P^0\omega_3\omega_4(s - \omega_1^2 - (\omega_2 + \omega_4)^2 - \omega_1(\omega_2 + 2\omega_4))E_3^3 \\
&- \omega_3((\omega_2 + \omega_4)\omega_1^4 + (\omega_2 + \omega_4)(\omega_2 + 2(\omega_3 + \omega_4))\omega_1^3 + (\omega_2^3 + (4\omega_3 + 5\omega_4)\omega_2^2 + 2(\omega_3^2 + 5\omega_4\omega_3 + 3\omega_4^2)\omega_2 \\
&+ 2\omega_4(-s + \omega_3^2 + \omega_4^2 + 3\omega_3\omega_4))\omega_1^2 + (\omega_2^4 + (2\omega_3 + 3\omega_4)\omega_2^3 + 2(\omega_3^2 + 5\omega_4\omega_3 + 3\omega_4^2)\omega_2^2 \\
&+ 2\omega_4(s + 3\omega_3^2 + 3\omega_4^2 + 7\omega_3\omega_4)\omega_2 + 2\omega_4(\omega_3 + \omega_4)(\omega_4(2\omega_3 + \omega_4) - s))\omega_1 + \omega_4(-s + \omega_2^2 + 2\omega_3^2 + \omega_4^2 \\
&+ 2\omega_2\omega_3 + 2\omega_3\omega_4)((\omega_2 + \omega_4)^2 - s))E_3^2 + 2P^0\omega_3\omega_4(\omega_1^4 + (\omega_2 + 2(\omega_3 + \omega_4))\omega_1^3 + (\omega_2^2 + 2(\omega_3 + \omega_4)\omega_2 \\
&+ \omega_3^2 + \omega_4^2 + 4\omega_3\omega_4)\omega_1^2 + (\omega_2^3 + 2(\omega_3 + \omega_4)\omega_2^2 + (\omega_3^2 + 4\omega_4\omega_3 + \omega_4^2)\omega_2 + 2\omega_3\omega_4(\omega_3 + \omega_4))\omega_1 \\
&+ (\omega_2 + \omega_3)^2(\omega_2 + \omega_4)^2 - s(\omega_1^2 + (\omega_2 + 2\omega_3)\omega_1 + (\omega_2 + \omega_3)^2))E_3 + (\omega_1 + \omega_3)(\omega_2 + \omega_3)(((\omega_3 + \omega_4)\omega_2^2 \\
&+ (\omega_3^2 + 3\omega_4\omega_3 + 2\omega_4^2)\omega_2 + \omega_4((\omega_3 + \omega_4)^2 - s))\omega_1^3 + (\omega_2 + \omega_3 + 2\omega_4)((\omega_3 + \omega_4)\omega_2^2 \\
&+ (\omega_3^2 + 3\omega_4\omega_3 + 2\omega_4^2)\omega_2 + \omega_4((\omega_3 + \omega_4)^2 - s))\omega_1^2 + ((\omega_3^2 + 3\omega_4\omega_3 + 2\omega_4^2)\omega_2^3 + (\omega_3^3 + 6\omega_4\omega_3^2 + 10\omega_4^2\omega_3 \\
&+ 5\omega_4^3 - s\omega_4)\omega_2^2 + \omega_4(3\omega_3 + 4\omega_4)((\omega_3 + \omega_4)^2 - s)\omega_2 + \omega_4(s^2 - (\omega_3^2 + 4\omega_4\omega_3 + 2\omega_4^2)s \\
&+ \omega_4(\omega_3 + \omega_4)^2(2\omega_3 + \omega_4)))\omega_1 + (\omega_2 + \omega_3)\omega_4((\omega_2 + \omega_4)^2 - s)((\omega_3 + \omega_4)^2 - s))).
\end{aligned}
$$

$$\text{(C1)}$$

[1] S. Weinberg, Physica A (Amsterdam) **96**, 327 (1979).
[2] J. Gasser and H. Leutwyler, Nucl. Phys. **B250**, 465 (1985).
[3] U. G. Meissner, Rep. Prog. Phys. **56**, 903 (1993).
[4] V. Bernard, N. Kaiser, and U. G. Meissner, Int. J. Mod. Phys. E **4**, 193 (1995).
[5] A. Pich, Rep. Prog. Phys. **58**, 563 (1995).
[6] G. Ecker, Prog. Part. Nucl. Phys. **35**, 1 (1995).
[7] S. Scherer, Adv. Nucl. Phys. **27**, 277 (2003).
[8] V. Bernard, Prog. Part. Nucl. Phys. **60**, 82 (2008).
[9] A. Dobado and J. R. Pelaez, Phys. Rev. D **56**, 3057 (1997).
[10] J. A. Oller, E. Oset, and J. R. Pelaez, Phys. Rev. D **59**, 074001 (1999); **60**, 099906(E) (1999); **75**, 099903(E) (2007).
[11] J. A. Oller and E. Oset, Phys. Rev. D **60**, 074023 (1999).
[12] J. A. Oller and U. G. Meissner, Phys. Lett. B **500**, 263 (2001).
[13] J. A. Oller and E. Oset, Nucl. Phys. **A620**, 438 (1997); **A652**, 407(E) (1999).
[14] N. Kaiser, Eur. Phys. J. A **3**, 307 (1998).
[15] N. Kaiser, P. B. Siegel, and W. Weise, Nucl. Phys. **A594**, 325 (1995).
[16] V. E. Markushin, Eur. Phys. J. A **8**, 389 (2000).
[17] E. Oset and A. Ramos, Nucl. Phys. **A635**, 99 (1998).
[18] C. Garcia-Recio, M. F. M. Lutz, and J. Nieves, Phys. Lett. B **582**, 49 (2004).
[19] D. Jido, J. A. Oller, E. Oset, A. Ramos, and U. G. Meissner, Nucl. Phys. **A725**, 181 (2003).
[20] C. Garcia-Recio, J. Nieves, and L. L. Salcedo, Phys. Rev. D **74**, 034025 (2006).
[21] T. Hyodo, S. I. Nam, D. Jido, and A. Hosaka, Phys. Rev. C **68**, 018201 (2003).
[22] E. E. Kolomeitsev and M. F. M. Lutz, Phys. Lett. B **585**, 243 (2004).
[23] S. Sarkar, E. Oset, and M. J. Vicente Vacas, Nucl. Phys. **A750**, 294 (2005); **A780**, 90 (2006).
[24] M. F. M. Lutz and E. E. Kolomeitsev, Nucl. Phys. **A730**, 392 (2004).
[25] L. Roca, E. Oset, and J. Singh, Phys. Rev. D **72**, 014002 (2005).
[26] V. K. Magas, E. Oset, and A. Ramos, Phys. Rev. Lett. **95**, 052301 (2005).
[27] L. S. Geng, E. Oset, L. Roca, and J. A. Oller, Phys. Rev. D **75**, 014017 (2007).
[28] E. E. Kolomeitsev and M. F. M. Lutz, Phys. Lett. B **582**, 39 (2004).
[29] J. Hofmann and M. F. M. Lutz, Nucl. Phys. **A733**, 142 (2004).
[30] F. K. Guo, P. N. Shen, H. C. Chiang, and R. G. Ping, Phys. Lett. B **641**, 278 (2006).
[31] D. Gamermann, E. Oset, D. Strottman, and M. J. Vicente Vacas, Phys. Rev. D **76**, 074016 (2007).
[32] A. Martinez Torres, K. P. Khemchandani, and E. Oset, Phys. Rev. C **77**, 042203 (2008).
[33] A. Martinez Torres, K. P. Khemchandani, L. S. Geng, M. Napsuciale, and E. Oset, Phys. Rev. D **78**, 074031 (2008).
[34] L. Alvarez-Ruso and V. Koch, Phys. Rev. C **65**, 054901 (2002).
[35] R. Molina, D. Nicmorus, and E. Oset, Phys. Rev. D **78**, 114018 (2008).
[36] M. Bando, T. Kugo, S. Uehara, K. Yamawaki, and T. Yanagida, Phys. Rev. Lett. **54**, 1215 (1985).
[37] M. Bando, T. Kugo, and K. Yamawaki, Phys. Rep. **164**, 217 (1988).
[38] C. Amsler et al. (Particle Data Group), Phys. Lett. B **667**, 1 (2008).
[39] H. Nagahiro, J. Yamagata-Sekihara, E. Oset, and S. Hirenzaki, arXiv:0809.3717.
[40] L. S. Geng and E. Oset, arXiv:0812.1199.
[41] A. I. Titov, B. Kampfer, and B. L. Reznik, Eur. Phys. J. A **7**, 543 (2000).
[42] A. I. Titov, B. Kampfer, and B. L. Reznik, Phys. Rev. C **65**, 065202 (2002).
[43] D. V. Bugg, Eur. Phys. J. C **52**, 55 (2007).
[44] S. Uehara (private communication).
[45] M. Albaladejo and J. A. Oller, Phys. Rev. Lett. **101**, 252002 (2008).
[46] M. Ablikim et al., Phys. Lett. B **642**, 441 (2006).
[47] M. Ablikim et al. (BES Collaboration), Phys. Lett. B **603**, 138 (2004).
[48] J. Z. Bai et al. (BES Collaboration), Phys. Lett. B **472**, 200 (2000).
[49] J. E. Augustin et al. (DM2 Collaboration), Nucl. Phys. **B320**, 1 (1989).
[50] M. E. B. Franklin et al., Phys. Rev. Lett. **51**, 963 (1983).
[51] J. Burmester et al. (PLUTO Collaboration), Phys. Lett. **72B**, 135 (1977).
[52] B. Jean-Marie et al., Phys. Rev. Lett. **36**, 291 (1976).
[53] P. Achard et al. (L3 Collaboration), Phys. Lett. B **568**, 11 (2003).
[54] P. Achard et al. (L3 Collaboration), Phys. Lett. B **597**, 26 (2004); **604**, 48 (2004); **615**, 19 (2005).
[55] I. V. Anikin, B. Pire, and O. V. Teryaev, Phys. Lett. B **626**, 86 (2005).
[56] H. Albrecht et al. (ARGUS Collaboration), Z. Phys. C **50**, 1 (1991).
[57] A. Filippi et al. (OBELIX Collaboration), Phys. Lett. B **495**, 284 (2000).
[58] J. A. Oller, E. Oset, and A. Ramos, Prog. Part. Nucl. Phys. **45**, 157 (2000).
[59] J. A. Oller (private communication).